frontiers in Earth Science

ORIGINAL RESEARCH
published: 28 January 2020
doi: 10.3389/feart.2019.00353

Erosional and Tectonic Evolution of a Retroarc Orogenic Wedge as Revealed by Sedimentary Provenance: Case of the Oligocene – Miocene Patagonian Andes

Joel S. Leonard[1,2], Julie C. Fosdick[3] and Rebecca A. VanderLeest[3]*

[1] School of Earth and Space Exploration, Arizona State University, Tempe, AZ, United States, [2] Department of Earth and Atmospheric Sciences, Indiana University, Bloomington, IN, United States, [3] Department of Geosciences, University of Connecticut, Storrs, CT, United States

OPEN ACCESS

Edited by:
David Mark Hodgson, University of Leeds, United Kingdom

Reviewed by:
Joel Saylor, The University of British Columbia, Canada
Brian K. Horton, The University of Texas at Austin, United States
Emily Finzel, The University of Iowa, United States

***Correspondence:**
Joel S. Leonard
joel.leonard@asu.edu

Specialty section:
This article was submitted to Sedimentology, Stratigraphy, and Diagenesis, a section of the journal Frontiers in Earth Science

Received: *16 August 2019*
Accepted: *18 December 2019*
Published: *28 January 2020*

Citation:
Leonard JS, Fosdick JC and VanderLeest RA (2020) Erosional and Tectonic Evolution of a Retroarc Orogenic Wedge as Revealed by Sedimentary Provenance: Case of the Oligocene – Miocene Patagonian Andes. Front. Earth Sci. 7:353. doi: 10.3389/feart.2019.00353

Sedimentary provenance techniques have been widely applied in foreland basin settings to understand tectonic and magmatic processes by tracking the exposure and erosion of distinct sediment source areas through time. We present a case example from the Magallanes-Austral retroarc foreland basin of Chile and Argentina (51°30'S), where modal sandstone and conglomerate compositional data, detrital zircon U-Pb geochronology, and sedimentology data from the Oligocene-Miocene Río Guillermo Formation document a change in source areas during an important stage of orogenic development. In particular, our results from the ∼24.3–21.7 Ma Río Guillermo Formation record an abrupt shift from transitional to undissected arc provenance that indicate rejuvenated magmatism within the contemporary arc. Minor components of lithic grains suggest a subordinate source of recycled sediments that we interpret may have been derived from the intervening external fold-and-thrust belt, rather than directly from sources in the hinterland thrust domain. Detrital zircon U-Pb geochronology data show mostly Neogene (∼20–40 Ma) and Cretaceous (∼70–110 Ma) age groups, with minor amounts of Jurassic (∼145–155 Ma), and Paleozoic (∼260–540 Ma) age groups, which are consistent with a syndepositional arc and recycled external fold-and-thrust belt sources. Stratigraphic data suggest a vegetated, channelized braidplain environment developed above an erosional unconformity with the underlying shallow-marine Río Turbio Formation. Upsection, the Río Guillermo Formation locally transitions to a low-energy, organic-rich floodplain setting located within the upper reaches of a fluvial-tidal transition zone of the coastal plain, and the uppermost part of the formation is characterized by a coarse-grained sandy channelized braidplain environment along the foreland basin margin. Moderate sediment accumulation rates and coastal plain

progradation during this period is consistent with sustained sediment flux from the Patagonian Andes and tectonic subsidence along the basin margin. Taken collectively, we propose that the abrupt provenance shift dominantly records erosion of the rejuvenated mafic volcanic arc, despite coeval changes in orogenic wedge dynamics brought about by increased plate convergence rates that drove uplift of the intervening external-fold-and-thrust belt along reactivated deep-seated high-angle basin structures.

Keywords: foreland basins, sedimentary provenance, patagonian andes, magallanes-austral basin, cenozoic

INTRODUCTION

In Cordilleran systems, crustal thickening caused by retroarc upper plate shortening, batholith emplacement, and arc volcanism build topography, while surface processes act to erode and redistribute sediments to the foreland basin. The surface evolution of convergent orogens is archived in the sedimentary deposits of their companion foreland basins, but unlocking this archive requires discerning tectonic signals from climatic or eustatic signals that control the depositional environments and composition of basin infill. Thus, considerable research has been devoted to identifying diagnostic signals of tectonics, climate, and eustasy in sedimentary deposits (e.g., Posamentier et al., 1988; Jordan and Flemings, 1991; Heller et al., 1993, 2001; Paola, 2000; Armitage et al., 2011; Romans et al., 2016). The location and magnitude of upper plate shortening and rock uplift will dictate the lithology of potential source areas within the orogen. The development of orogenic wedges may follow Coulomb wedge theory as phases of internal deformation or self-similar growth in response to changes in the frictional properties and physical characteristics of the wedge over time, such as pore pressure, depth and geometry of basal detachment, and surface slope (Davis et al., 1983; Dahlen, 1984; DeCelles and Mitra, 1995; Horton, 1999; Willett, 1999). However, in orogens with reactivated high-angle structures (e.g., Hilley et al., 2005; Mora et al., 2006; Saylor et al., 2012), the patterns of deformation and erosion may reflect vertical uplift and exhumation rather than high rates of internal shortening across the orogenic wedge.

In the absence of direct measurements of deformation, sediment provenance can shed light on erosion of different source areas that may respond to changes in orogenic wedge behavior. Pulses of coarse-grained sediments in foreland basins are commonly interpreted within the context of increased sediment supply from thrust-generated topography, and/or increased precipitation and erosion (Burbank et al., 1988; Heller et al., 1988; Paola et al., 1992; Garcia-Castellanos et al., 2002; Allen and Heller, 2011; Armitage et al., 2011). Abrupt shifts in sediment provenance at geologic timescales can be an indication of tectonic reconfiguration of upland source areas (Horton et al., 2004). Thus, the timing, duration, and sedimentary character of the progradational units bear on the tectonic history of an orogenic system.

We explore the sedimentary provenance and sedimentology of the latest Oligocene-early Miocene basin record in the Southern Patagonian Andes (**Figure 1**), which preserves coarse-grained deposition during the early stages of a regionally important phase of mountain-building and changes in orogenic wedge dynamics. The Magallanes–Austral retroarc foreland basin lies on the eastern flank of the Patagonian Andes at the southern tip of the South American continent (**Figure 1**). This foreland basin and fold-and-thrust belt records a long-lived orogenic system with a major phase of mountain-building in the Late Cretaceous (∼100–88 Ma) following closure and inversion of the Rocas Verdes Basin and arc-continent collision (Calderón et al., 2016). At the latitude of our study area, this depocenter was a predominantly longitudinal marine depositional system that derived much of its sediment from the continental Patagonian and Fuegian Andes (Fildani et al., 2008; Romans et al., 2011). Thrust front advancement during Paleogene time and progressive deepening of the basal sole-out detachment depth in latest Oligocene – early Miocene time (Fosdick et al., 2011) promoted an eastward shift of the foreland deposition and a transition to transverse sediment routing (Biddle et al., 1986; Fosdick et al., 2011). These younger phases of Cenozoic orogenesis are broadly coeval with major mountain building, crustal shortening, and basin subsidence in the Central and Northern Andes (e.g., Horton, 2018); however, the magnitude of shortening and preserved basin record is considerably less in the Magallanes-Austral Basin (Fosdick et al., 2011).

Here, we investigate the Chattian-Aquitanian Río Guillermo Formation from the Magallanes-Austral Basin (**Figure 1**), and by comparison with potential source areas and provenance studies from underlying basin strata, answer the following questions: (1) What were the primary sediment sources of the Río Guillermo Formation? (2) How are the coarse-grained progradational deposits linked to the thrusting history and changes in upland sediment-source paleogeography? Our findings constrain the sources of sediment and stratigraphic stacking patterns during reactivation of deep-seated faulting and regional uplift of the Patagonian fold-and-thrust belt. These findings capitalize on new age constraints for the timing of Cenozoic (Maastrichtian through early Miocene) sedimentation in the Magallanes-Austral Basin (Fosdick et al., 2011, 2019), and reinforce causal linkages between changes in sediment routing and a structural reorganization of the Patagonian fold-and-thrust belt (**Figure 1B**). Our work on the Río Guillermo Formation, specifically, provides new detailed sedimentology and provenance data that add further context for regional exhumation and magmatic evolution histories that, taken

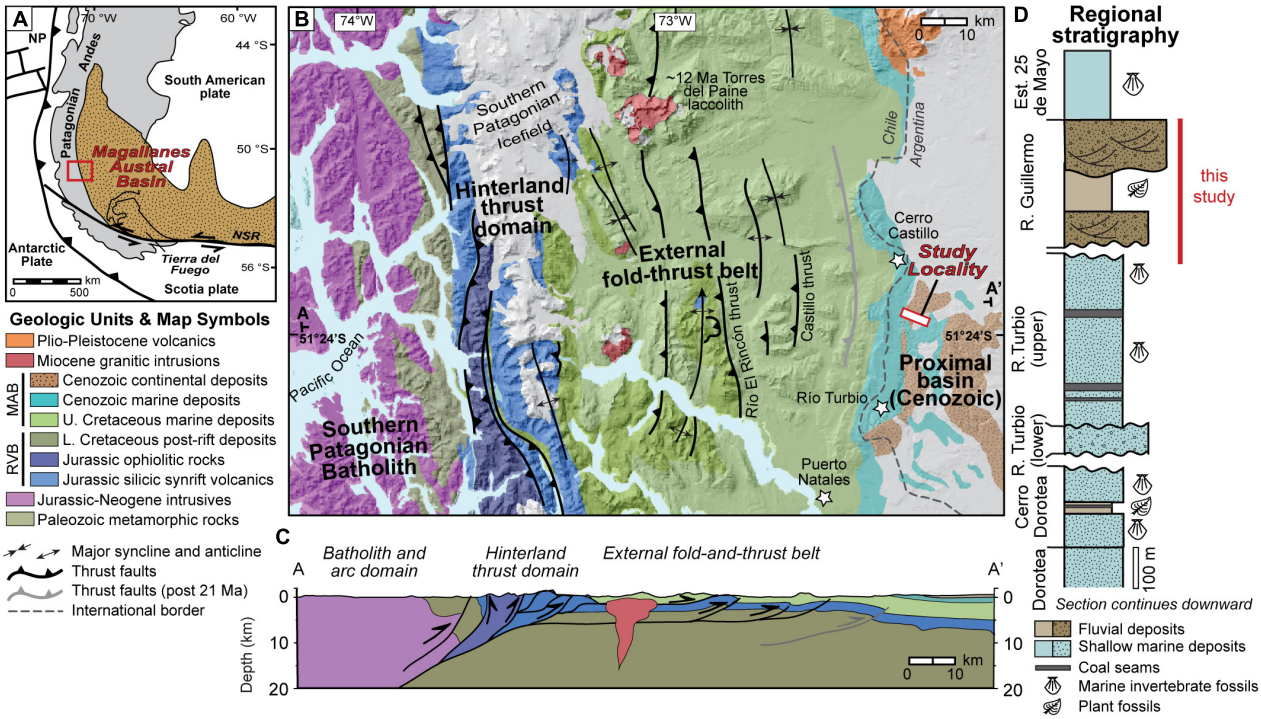

FIGURE 1 | (A) Location of the Patagonian Andes retroarc orogenic belt and foreland basin system. NP, Nazca plate; NSR, North Scotia Ridge. **(B)** Geologic map compiled from Malumián et al. (2000), SERNAGEOMIN (2003), and Fosdick et al. (2011). The hinterland thrust domain includes faulted and folded rocks of Jurassic Sarmiento Ophiolitic Complex and Tobífera Formation. The external fold-and-thrust belt comprises the Zapata, Punta Barrosa, Cerro Toro, Tres Pasos, and Dorotea formations. MAB, Magallanes-Austral Basin; RVB, Rocas Verdes Basin. **(C)** Simplified regional cross-section showing major structural features of the Patagonian Andes (modified from Fosdick et al., 2011, 2013). **(D)** Regional stratigraphy of the study area showing Upper Cretaceous – Neogene strata (adapted from Fosdick et al., 2019). See text for discussion.

together, contribute to a better understanding of coupled foreland basin and orogenic processes.

GEOLOGIC SETTING AND PREVIOUS WORK

Tectonic and Sedimentary History of the Magallanes-Austral Basin

The Magallanes-Austral retroarc foreland basin of Chile and Argentina is situated at the southernmost tip of South America adjacent to the Patagonian and Fuegian Andes orogenic belt (Ghiglione et al., 2016; **Figure 1A**). Prior to its transition to foreland depocenter in the Early Cretaceous, this region was occupied by the Rocas Verdes backarc basin that formed in the Jurassic as a result of the tectonic break-up of Gondwana (Dalziel et al., 1974; Wilson, 1991; Fildani and Hessler, 2005; Calderón et al., 2016). Backarc spreading culminated in the genesis of attenuated pseudo-oceanic crust and deep marine sedimentary conditions (Dalziel et al., 1974; de Wit and Stern, 1981; Fildani and Hessler, 2005). Initiation of subduction of the Farallon-Nazca plate beneath South America and compression from the west in the Early Cretaceous led to closure of the Rocas Verdes backarc and the conclusion of this pre-foreland extensional phase (Calderón et al., 2012, 2016). However, pre-foreland structural remnants and weakened crust produced during this time are thought to be important factors controlling sedimentation patterns in the basin during the Late Cretaceous and the opening of the South Atlantic Ocean (Romans et al., 2010; Malkowski et al., 2017).

Extensive research over several decades has characterized early foreland development of a narrow foredeep trough and protracted deep marine sedimentary conditions, followed by southward axial progradation and infilling by slope-shelf and deltaic systems from the Late Cretaceous through early Cenozoic (Macellari et al., 1989; Fildani and Hessler, 2005; Hubbard et al., 2008; Romans et al., 2011; Malkowski et al., 2017; Sickmann et al., 2019). Crustal shortening estimates suggest that at least 20–27 km of shortening across the narrow fold-and-thrust belt occurred during this time (Fosdick et al., 2011). Shallow to marginal marine, deltaic, and estuarine sedimentary environments persisted in the basin through the Paleogene (Malumián and Caramés, 1997; Rodríguez Raising, 2010; Schwartz and Graham, 2015), and by Eocene – Oligocene time growth and encroachment of the Patagonian external fold-and-thrust belt resulted in consistent eastward (i.e., transverse) sediment dispersal (Biddle et al., 1986). Few constraints on the timing and magnitude of Paleogene crustal shortening are available, but estimates based on cross-cutting relationships

suggest ∼6.5 km of shortening occurred prior to 29 Ma (Fosdick et al., 2011). Early Eocene subduction of the Aluk-Farallon spreading ridge (Cande and Leslie, 1986; Breitsprecher and Thorkelson, 2009) resulted in a hiatus of arc volcanism that lasted from middle Eocene – latest Oligocene time (Ramos, 1989; Hervé et al., 2007), but produced regionally extensive plateau basalts (Ramos and Kay, 1992), and may have caused broad regional uplift that enhanced a basin-wide Paleogene unconformity within the foreland succession (Biddle et al., 1986; Fosdick et al., 2015; Schwartz et al., 2016; George et al., 2019).

Late Oligocene time marked a switch in the characteristic style of foreland deformation, from dominantly thin-skinned to high-angle basement-cored thrusting with less retroarc shortening (∼3–4 km) across the fold-and-thrust belt (Fosdick et al., 2011), that is followed closely by deposition of the first exclusively terrestrial and fluvial systems at this latitude in the earliest Miocene (Fosdick et al., 2019). The switch to basement-cored thrusting (**Figure 1C**) is generally attributed to more rapid and trench-normal convergence on the western margin of South America ∼27 Ma (Fosdick et al., 2011; Somoza and Ghidella, 2012; Ghiglione et al., 2016), although other authors suggest that far-field effects relating to growth of the North Scotia Ridge, and Tierra del Fuego to the south ∼23 Ma (Cunningham et al., 1995; Eagles and Jokat, 2014) may have also played a role (Lagabrielle et al., 2009; Fosdick et al., 2013). The seismically imaged basement thrusts are interpreted to be reactivated high-angle extensional structures inherited from the predecessor Rocas Verdes Basin (Fosdick et al., 2011). Terrestrial sedimentary conditions are succeeded by a brief, but regionally extensive marine incursion and return to shallow marine conditions across much of the basin in early Miocene time (Malumián and Caramés, 1997). Recently, the dominant control on the extent and magnitude of basin flooding has been interpreted as propagation of the Patagonian Andean thrust front and associated increase in flexural subsidence (Fosdick et al., 2019). Key to this interpretation is revised chronology of the upper part of the Río Turbio Formation and overlying Río Guillermo Formation, which are as young as latest Priabonian through middle Chattian (36.6–26.6 Ma), and latest Chattian through Aquitanian (24.3–21.7 Ma), respectively (Fosdick et al., 2011, 2019). Finally, deposition of the synorogenic Santa Cruz Formation (∼18–14) Ma record coeval coarse-grained sedimentation, surface uplift, and continental sedimentation across the Patagonian foreland (e.g., Blisniuk et al., 2005; Ramos and Ghiglione, 2008) prior to passage of the Chile Triple Junction at this latitude (Gorring et al., 2003; Kay et al., 2004; Breitsprecher and Thorkelson, 2009). Opening of a slab window resulting from this later ridge collision is associated with regional uplift of the Patagonian foreland and inversion of the Magallanes-Austral Basin (Guillaume et al., 2009, 2013; Fosdick et al., 2011).

Previous Work on Río Guillermo Formation

The Río Guillermo Formation is the first exclusively terrestrial sedimentary unit at this latitude (∼51°S) (Hünicken, 1955; Malumián and Caramés, 1997; Rodríguez Raising, 2010), but is scarcely exposed at the surface and has been the subject of widely varying interpretations of both its age and significance relating to the greater basin development. The base of the Río Guillermo Formation in the study region is characterized by an erosional unconformity with ∼20–30 cm of channelized pebble-to-cobble conglomerate scoured into the underlying mudstone beds of the Río Turbio Formation (**Figure 1D**). It is generally composed of conglomerate, sandstone, and mudstone interpreted to be fluvial in origin, minor coal horizons, and notably containing abundant silicified tree trunks (Malumián and Caramés, 1997). Sandstones are composed largely of volcanic detritus, suggesting the potential for arc-related provenance (Manassero, 1990). Early work correlated this unit with the coeval Río Leona Formation that has similar characteristics and is more regionally exposed, and suggested an Oligocene – Miocene age (Riccardi and Rolleri, 1980; Russo et al., 1980). However, later work assigns early Eocene – early Oligocene ages on the basis of paleontological assemblages (Malumián and Caramés, 1997; Malumián et al., 2000; Rodríguez Raising, 2010; Malumián and Náñez, 2011; Pearson et al., 2012). This discrepancy in age assignments had led to disperate associations with Eocene – Oligocene marine transgressions and climatic optima (Malumián and Caramés, 1997; Malumián et al., 2000; Malumián and Náñez, 2011). Rodríguez Raising (2010) conducted a sequence stratigraphic analysis and documented an overall upward increase in rate of basin accommodation generation, superimposed by cyclic phases of aggradation, and erosion linked generally to phases of deformation.

As part of a regional study on the kinematic history of faulting and sedimentaton across the Patagonian Andes, Fosdick et al. (2011) reported a zircon U-Pb SHRIMP age from an interbeded tuff at the top of the Río Guillermo Formation, suggesting the top of the unit was as young as 21.7 Ma. More recently, Fosdick et al. (2019) provided new estimates on the timing of sedimentaton for the whole Cenozoic basin succession in our study area – including the lower formationnal boundary of the Río Guillermo Formation – based on detrital zircon U-Pb geochronological data. These data establish a latest Chattian through Aquitanian age (∼24.3–21.7 Ma) for the Río Guillermo Formation and support the interpretation of contemporaneous deposition with previously recongnized faulting stages within the fold-and-thrust belt (later Stage IV and early Stage V faulting of Fosdick et al., 2011, 2019). This work provides detailed sedimentology, sandstone petrography, modal clast analysis, and additional detrital zircon U-Pb geochronology of the Río Guillermo Formation.

Characteristic Source Areas in the Patagonian Andes

New provenance data from the upper Eocene - lower Miocene Magallanes-Austral basinfill at ∼51°S capture changes in sediment composition and interpreted changes in source areas. Here we summarize the age, lithology, and tectonic association of potential sources [see Romans et al. (2010), Fosdick et al. (2015),

Schwartz et al. (2016), Daniels et al. (2017), George et al. (2019), Sickmann et al. (2019)] for recent work of the detrital zircon geochronology from the Cretaceous basin fill).

(1) The Patagonian continental basement comprises Paleozoic metamorphic units exposed as wall rocks to the Mesozoic-Neogene batholith and within thrust slices in the hinterland thrust domain (**Figure 1B**). At the latitude of the study area, these rocks include the Paleozoic Eastern Andean Metamorphic Complex (EAMC), a variably deformed and metamorphosed complex of greenschist grade turbiditic and minor intercalated marl successions and metabasite flows, and localized areas of higher metamorphic grade rocks (Hervé et al., 2003, 2008; Calderón et al., 2016).

(2) Generally east of the Paleozoic metamorphic basement, the hinterland thrust domain is characterized by Upper Jurassic (∼140–160 Ma) metarhyolitic Tobífera Formation and ophiolitic rocks of the Rocas Verdes Basin (**Figure 1B**). These rocks represent the quasi-oceanic and attenuated continental lithosphere of the backarc basin floor, prior to closure of the basin during arc-continent collision and inversion of the retroarc basin during initiation of the Magallanes-Austral foreland basin phase. Today, the modern drainage divide resides along the Tobífera duplex structures constructed from thrust stacks of the Tobífera Formation (**Figure 1C**). Post-rifting thermal sag and incipient foreland basin sedimentation are preserved in the upper Jurassic – lower Cretaceous Zapata Formation.

(3) The Paleozoic basement and Jurassic hinterland thrust domain is intruded by the Late Jurassic – Neogene Southern Patagonian Batholith (SPB), which preserves the root of the Late Jurassic – Neogene magmatic arc system (**Figures 1B,C**). There are three primary recognized Cretaceous episodes of plutonic emplacement (144–137, 136–127, and 126–75 Ma), followed by early Paleogene (67–40 Ma), and Neogene (25–15 Ma) episodes (Hervé et al., 2007). Some of the Miocene granitic intrusions locally intrude the external fold-and-thrust belt (described below), including the ∼26 Ma Cerro Donoso pluton, ∼15.4 Ma Cerro Balmaceda pluton, and ∼12.5 Ma Torres del Paine Intrusive Complex (Michel et al., 2008; Sánchez et al., 2008; Ramírez de Arellano et al., 2012). Rocks are generally composed of granodiorite, tonalite, and granite, with minor isolated gabbroic intrusions.

(4) East of the Paleozoic-Jurassic basement thrust domain, the Cretaceous – Neogene external fold-and-thrust belt consists of Cenomanian-Paleocene retroarc foreland basin marine mudstone, siltstone, and sandstone deposited in submarine channel-fill deposits of the Punta Barossa, Cerro Toro, Tres Pasos, and Dorotea Formations (**Figure 1B**). In general, these rocks are characterized by *dissected arc* provenance, with dominant sources from the SPB, hinterland thrust domain, and Paleozoic metamorphic basement (Fildani and Hessler, 2005; Hubbard et al., 2008; Romans et al., 2010; Schwartz et al., 2016). Structural style includes both thin-skinned and thick-skinned deformation. Importantly, the eastern leading edge of the external thrust belt (i.e., the Río El Rincon and Castillo thrust sheets) sedimentary succession would have constituted the deformation front during deposition of the upper Río Turbio and Río Guillermo formations (Fosdick et al., 2011; **Figure 1C**).

Based on structural style and characteristic domains of deformation (Ghiglione et al., 2010; Fosdick et al., 2011), we refer separately to these source areas as the basement domain (Paleozoic basement and Mesozoic SPB), the hinterland thrust domain (Rocas Verdes Basin floor, high-angle shear zones, and thin-skinned detachments within the basal Tobífera metavolcanic units), and the external fold-and-thrust belt (thin-skinned deformation superimposed by reactivated basement faults).

METHODS AND RESULTS

Our analysis consists of a stratigraphic section of the Río Guillermo Formation that records detailed provenance during incipient terrestrial sedimentation at this latitude. Sample details including geographic locations, position in measured sections, and type of analysis are summarized in **Table 1**.

Oligocene-Miocene Sedimentology and Stratigraphy

We focused on the outcrop exposures of the Río Guillermo Formation and underlying Río Turbio Formation in the Estancia Cancha Carrera, east of the Chile-Argentina international border (**Figure 1B**). Here, the outcrops are variably well-exposed in the stream valley of the modern Río Guillermo and form a series of gently east-dipping exposures along the incised river valley (**Figures 2A,E**). Locally, the Neogene deposits are disconformably overlain by Pleistocene glaciofluvial deposits and have deep soil horizons developed at the top of hillslope outcrops, thus limiting exposure to valley walls. The limited extent of high-quality rock exposure along the Patagonian foothills precludes a more extensive three-dimensional analysis of stratigraphic architecture, so we leverage high-resolution vertical information and sampling from this type locality of this stratigraphic level (Hünicken, 1955; Malumián et al., 2000). We measured approximately 340 m, locally constituting the full stratigraphic thickness of the fluvial Río Guillermo Formation. Paleocurrent measurements were taken from imbricated clasts, limbs of trough cross-beds, and orientations of petrified tree logs preserved in channel deposits, then corrected for 15°E regional dip. We characterize three subunits based on distinct changes in sedimentary facies assemblages (**Figure 3**). Sedimentary facies codes (**Table 2**) in the following unit descriptions are from Miall (1978, 2006). We make a distinction between "coarse-grained" and "fine-grained" depositional intervals such that coarse-grained refers to sand grain-sizes and larger, which in most cases herein is inferred to represent bedload deposition in an active channel.

Unit 1 is ∼95 m thick and consists of cliff-forming medium- to thick-bedded, trough cross-stratified, granule-to-cobble conglomerate (*Gt* and *Gh*). The base of the unit

TABLE 1 | Locality information for clast counts, sandstone petrography, and detrital zircon U-Pb LA-ICPMS samples.

Sample type	Sample	Formation	Latitude (°S)	Longitude (°W)	Elevation (m)	Stratigraphic Height (m)	Calculated MDA (Ma ± 2σ)
Conglomerate clast count	CCS3-PC2	Río Guillermo	51.30992	72.20304	405	271.5	
	CCS3-PC1	Río Guillermo	51.31000	72.20271	371	258	
	CCS2-PC2	Río Guillermo	51.31316	72.21686	379	91	
	CCS1-PC3	Río Guillermo	51.31308	72.22132	393	68	
	CCS1-PC1	Río Guillermo	51.31260	72.22176	358	17.5	
Sandstone petrography	15CCS307	Río Guillermo	51.30823	72.19668	403	336	
	15CCS305	Río Guillermo	51.30820	72.19702	391	321	
	15CCS304	Río Guillermo	51.30989	72.20073	381	300	
	15CCS303	Río Guillermo	51.30974	72.20173	386	276	
	15CCS302	Río Guillermo	51.31009	72.20272	395	270	
	15CCS301	Río Guillermo	51.31002	72.20271	375	263.5	
	15CCS212	Río Guillermo	51.31335	72.21058	348	119	
	15CCS108	Río Guillermo	51.31356	72.22148	389	69.5	
	15CCS107	Río Guillermo	51.31300	72.22132	406	65	
	15CCS106	Río Guillermo	51.31298	72.22125	371	52	
	15CCS104	Río Guillermo	51.31270	72.22145	377	31.5	
	15CCS102	Río Guillermo	51.31261	72.22161	355	17.5	
	15CCS101	Río Guillermo	51.31249	72.22168	348	3.5	
	15RTDZ01*	Río Turbio (upper)	51.30919	72.21978	334	−30	
	14RTDZ-7*	Río Turbio (upper)	51.29761	72.23581	349	−60	
	14RTDZ-8*	Río Turbio (upper)	51.29667	72.23819	282	−90	
Detrital Zircon	JCF09-237B‡	Río Guillermo	51.30338	72.18670	389	343	22.8 ± 0.2 (*n* = 65)
	15CCS306	Río Guillermo	51.30816	72.19702	381	321	23.0 ± 0.3 (*n* = 11)
	15CCS302	Río Guillermo	51.31009	72.20272	395	270	22.7 ± 0.3 (*n* = 16)
	15CCS210	Río Guillermo	51.31315	72.21645	380	94	24.6 ± 0.5 (*n* = 7)
	15CCS105	Río Guillermo	51.31296	72.22133	383	41.5	
	RT28DZ6‡	Río Guillermo	51.31163	72.22042	323	1	24.3 ± 0.6 (*n* = 8)
	RT28DZ5‡	Río Turbio (upper)	51.31373	72.21932	349	−1	26.6 ± 0.2 (*n* = 5)
	RT28DZ7‡*	Río Turbio (upper)	51.29761	72.23581	349	−60	35.4 ± 0.2 (*n* = 45)
	RT28DZ8‡*	Río Turbio (upper)	51.29667	72.23819	282	−90	36.6 ± 0.3 (*n* = 65)

‡*Samples from Fosdick et al. (2019).* **Approximate stratigraphic position in measured section.*

is the erosional contact with the underlying fine-grained Río Turbio Formation. Channelized bases are moderately erosive and marked by imbricated basal lag deposits, meter-scale, sand-filled channel cuts, and abundant petrified wood fragments (**Figures 2A–D**, **3**). Coarse-grained intervals increase in abundance and thickness upsection from ∼6–8 m to ∼12 m thick at the top of the unit (**Figure 3**). These coarse-grained strata are interbedded with thin-bedded, organic rich fine-grained sandstone and siltstone, with rare lignite horizons (*St, Fl,* and *C)*. Fossil plant debris (leaf impressions, twigs) and burrows, predominantly vertical, are common in fine-grained beds. We interpret these deposits to record conglomeratic fluvial bedload and overbank deposition of gravel bars and bedforms in a vegetated braidplain environment. Basal contacts of the fine-grained intervals are generally sharp, with little or no evidence of upward-fining that would reflect waning flow in the bedload deposition (e.g., Miall, 2006), consistent with an avulsive fluvial system. Abundant and well-preserved fossilized wood and tree stumps in life position suggest high sedimentation rates, subsidence, and burial of the floodplain (**Figures 2C**, **3**).

Unit 2 is ∼160 m thick and consists dominantly of poorly exposed, weakly stratified, interbedded organic-rich mudstone and siltstone (**Figures 2E,G,H**, **3**). The deposits are fissile with crude lamination and range in color from yellow to brown, gray, and orange (*Fl)* (**Figure 2F**). Where preserved, bedding style within organic-rich mudstone and siltstone ranges from horizontal lamination to lenticular bedding (**Figures 2G,H**). Rare thin beds of very fine- to fine-grained, horizontally laminated or structureless sandstone (*Fl*), and trough cross-stratified granule conglomerate (*Gt*) are present, and have erosive or sharp basal contacts, interpreted as localized splay deposits (**Figure 3**). Fossilized leaf impressions and other floral elements are present, though we note the lack of observed marine invertebrate fauna compared to those observed in the underlying upper Río Turbio Formation (Sequence 9 of Rodríguez Raising, 2010). Our observations are limited to the exposures of the lower part of Unit 2, and we estimate an additional ∼75 m of covered section within the fine-grained, recessive interval, based on regional dip and basal contact of overlying coarse-grained deposits of Unit 3. This interval is correlated across the Cancha Carrera study area, suggesting lateral continuity of this depositional facies. We

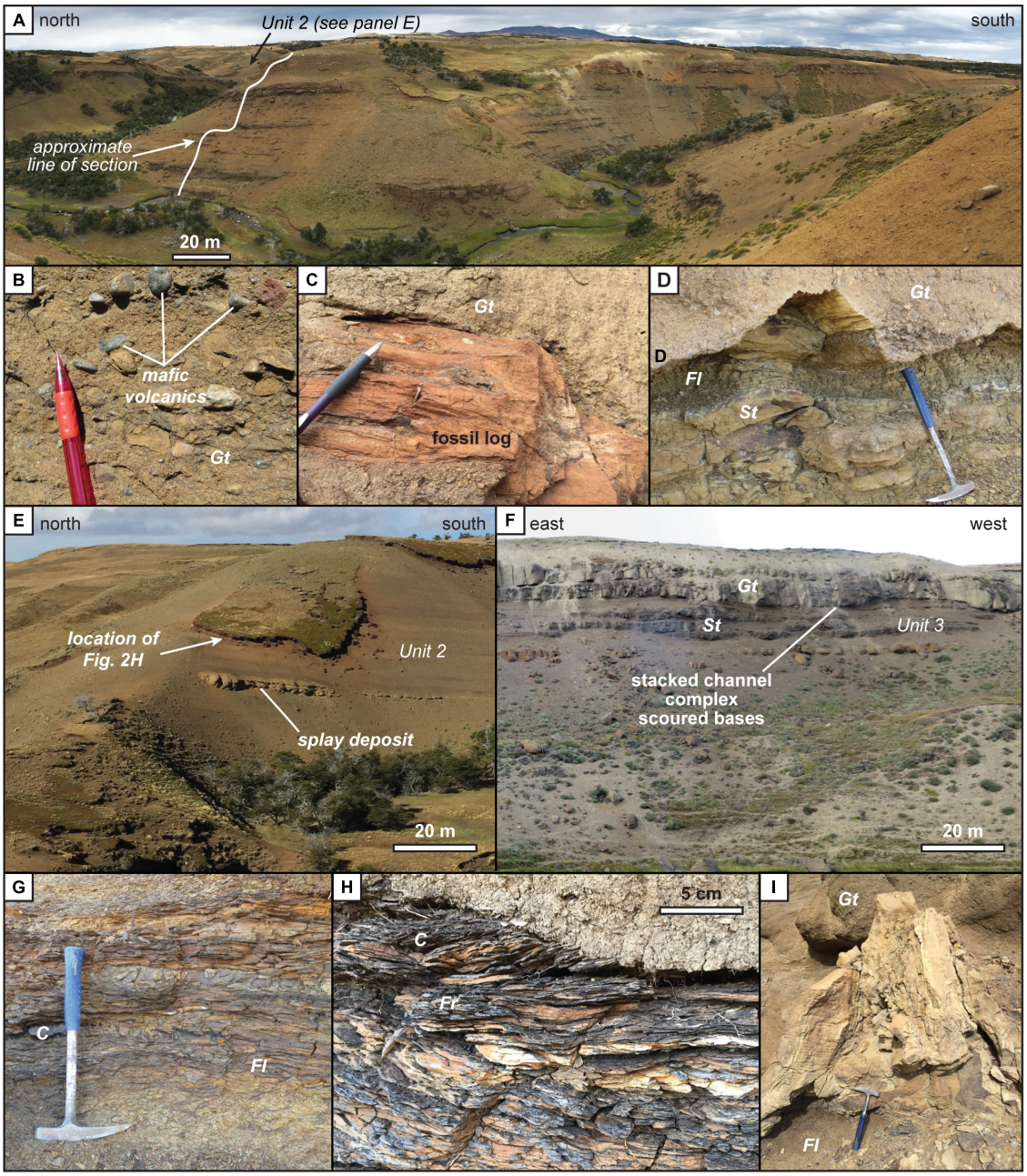

FIGURE 2 | Representative outcrops of the Río Guillermo Formation at the Cancha Carrera study area. **(A)** Panoramic basinward view of Unit 1 showing channelized *Gt* conglomerate and *St* sandstone and fine-grained, slope-forming strata (*Fl, C*). White line depicts location of part of the measured section in **Figure 3**. **(B)** Representative clasts from a *Gt* bed from Unit 1. **(C)** Petrified wood encased within *Gt* conglomerate in Unit 1. **(D)** Erosive base of channelized *Gt* strata into underlying fine-grained strata in Unit 1. **(E)** Panoramic basinward view of Unit 2 showing mostly interbedded mudstone and siltstone with sparse channelized *Gt*, *Gh*, *Gt* deposits. White line depicts location of part of the measured section. **(F)** Panoramic view of Unit 2 showing channelized *Gt* and *St* beds and recessive slope-forming *St* and *Sl* strata. **(G,H)** Fine-grained *St*, *Fl*, and *C* of Unit 2. **(I)** Fossilized tree trunk in life position, rooted in fine-grained *St and Fl* and buried by channel *Gt* deposits of Unit 3. See **Table 2** for lithofacies codes.

interpret deposits of Unit 2 to represent a sustained interval of low-energy, organic-rich floodplain deposition within the upper reaches of a fluvial-tidal transition zone of the coastal plain.

Unit 3 is ∼85 m thick and consists of sandstone, conglomerate, siltstone, mudstone, and minor lignite (**Figures 2F**, **3**). Conglomerate beds are generally trough cross-stratified with highly erosive basal contacts and occasionally have imbricate basal lags (*Gt, Gh,* and *St*), similar to Unit 1 (**Figures 2F**, **3**). Similar to the fine-grained depositional intervals within Unit 1, the siltstone and mudstone deposits are generally horizontally or

crudely ripple cross-laminated with sparse sandstone lenses (*Fl*) and rare lignite horizons (*C*). The distinguishing characteristic of Unit 3 is abundant thick-bedded, low angle trough cross-stratified sandstone that ranges in grain-size from very fine- to very coarse-grained. Planar cross-stratification and massive bedding are also present (*Sp, Sm)*, although are less abundant than trough cross-stratified bedding (**Figure 3**). Erosive or sharp basal contacts are most common between coarse- and fine-grained intervals, but upward fining bar forms are also present and are unique to Unit 3. Fossil logs and tree stumps in life position are present in both conglomerate and sandstone beds (**Figure 2I**). We interpret Unit 3 strata to have been deposited in a channelized, sandy fluvial braidplain environment. Preservation of bar forms and erosive conglomerate and sandstone deposits are consistent with channelized flow conditions, but the sharp depositional contacts between fine-grained overbank facies and underlying bedload deposits suggest an avulsive character to the fluvial system.

Taken together, increasing rates of vertical aggradation is apparent throughout the Río Guillermo Formation, as evidenced by distinct upsection changes in the character of active channel facies that either reflect increasing accommodation and/or sediment flux. Alternating coarse- and fine-grained intervals characteristic of the basal ∼100 m (Unit 1, **Figure 3**) are consistent with fluvial aggradation under accommodation limited conditions where preservation of sandstone in active channel deposits is poor (Miall, 2006). In contrast, active channel deposits in the uppermost ∼90 m (Unit 3, **Figure 3**) contain sandstone beds as well as similar fining-upward bar forms that indicate the rate of aggradation was relatively higher. Therefore, we interpret that a more continuous and expanded stratigraphy is represented higher in the section (Unit 3) than lower in the section (Unit 1), but both fundamentally reflect the same type of depositional system under differing accommodation or sediment flux conditions. The transition between these two depositional units is obscured by the thick accumulation of tidally influenced floodplain deposits (Unit 2) that we interpret reflect a combination of river avulsion and deepening along the basin margin coastal plain. The limited outcrop extent of the Río Guillermo Formation precludes evidence for any correlative in-channel deposits of equivalent age to Unit 2. Abundant tree trunks fossilized in life position, rooted in fine-grained floodplain deposits, and preserved by in-channel deposits suggests sedimentation rates were high throughout deposition of the full stratigraphic thickness (**Figure 3**), and more quantitative constraints on internal variations in sediment flux are not possible within the resolution of our data.

Modal Analysis of Conglomerate and Sandstone Compositions

We collected modal sandstone petrographic and conglomerate lithologic data from the Río Guillermo Formation and underlying upper Río Turbio Formation to track upsection changes in lithic grain compositions and diagnostic clast lithology that could be linked to potential source areas (**Figures 4**, **5**). Petrographic thin sections from 16 sandstone samples from the upper part of the Río Turbio and Río Guillermo formations were analyzed for quartz-feldspar-lithics framework mineralogy (QFL), lithic grain types (LmLvLs), single crystal phases, and cement composition (see **Figure 3** for sample locations in section). The three samples from the upper Río Turbio Formation were collected from Sequence 9 of Rodríguez Raising (2010). Samples were point-counted (for 400 grains) using the Gazzi-Dickinson method (after Ingersoll et al., 1984; Dickinson, 1985) using a Pelcon automated point counting system and a Leica DMZ2700 petrographic light microscope at Indiana University Bloomington. Grain parameters identified in these point counts are listed in the **Supplementary Table S1**, and recalculated data are provided in **Table 3**. Recalculated framework modal compositions were used to determine tectonic provenance (Dickinson and Suczek, 1979; Dickinson, 1985). Quartz-Feldspar-Lithics (i.e., QtFL and QmFLt) data from the upper Río Turbio and Río Guillermo formations were compared with published sandstone petrographic analyses of lower stratigraphic intervals and plotted on ternary diagrams, with tectonic fields as defined by Dickinson (1985). Refer to **Supplementary Table S1** for point counting grain classifications and **Supplementary Table S2** for raw point count data.

Ternary QFL, QmFLt, and LmLvLs plots of modal sandstone compositions from this study are shown in **Figure 4** accompanied by previously published samples from the underlying Punta Barrosa, Cerro Toro, Tres Pasos, and Dorotea formations (Fildani and Hessler, 2005; Valenzuela, 2006; Romans et al., 2010). These data reveal a long-term trend toward increasingly lithic-rich compositions upsection. In detail, the Punta Barrosa Formation records substantial contributions from metamorphic lithics, interpreted as incipient topographic uplift of the nascent orogen, and the Cerro Toro Formation records an increase in intermediate-to-felsic volcanic lithics, interpreted as unroofing of the Tobífera Formation in the hinterland thrust domain. Our data show a continuation of increasing lithic trend in the upper Río Turbio Formation culminating in a distinctly volcanic lithic-rich Río Guillermo Formation (**Figure 4**).

Detailed compositional data recorded from point counts are presented in **Figure 5**. In general, the upper Río Turbio Formation has an immature lithic-rich composition, particularly volcanic lithics. Relative abundances of quartz and lithic grains steadily increase upsection at the expense of feldspar and accessory minerals (**Figure 5B**). The Río Guillermo Formation is characterized by extreme compositional and textural immaturity, reflected in higher concentrations of labile mafic accessory minerals and volcanic lithic grains (**Figures 5B,C**). Quartz is sparse throughout, as is the proportion of metamorphic lithic grains relative to the upper Río Turbio Formation. Pyroxene also appears as an important mineral component. Finally, we note a consistent lack of sedimentary lithic grains in both units (**Figure 4**), but acknowledge this observation may be biased by preferential weathering. Notably, the upper Río Turbio Formation has a higher abundance of Lm compared to the Río Guillermo Formation (**Figure 4**).

Conglomerate compositions were determined by conducting *in situ* clast counts from five counting stations through the measured section of the Río Guillermo Formation, where

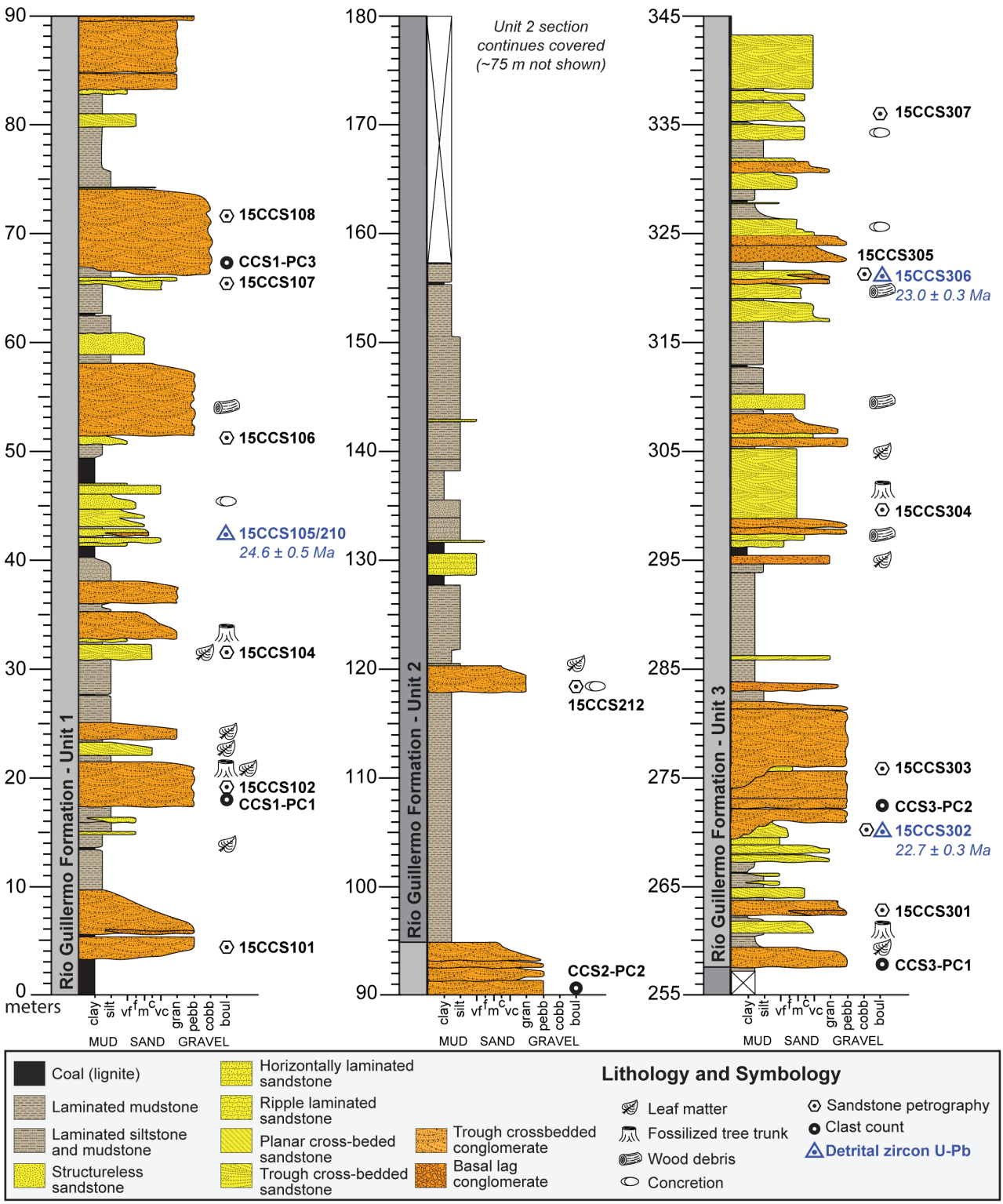

FIGURE 3 | Measured stratigraphic section of the Río Guillermo Formation at Cancha Carrera, Argentina, with sample locations for sandstone petrography, modal clast analysis, and detrital zircon U-Pb geochronology. We subdivide the formation into three major units based on sedimentology and stratigraphic architecture. Maximum depositional ages (blue triangles) interpreted from the detrital zircon U-Pb data are reported at 2σ. See text for detailed descriptions. Locations of measured section: Base 51.31259°S, 72.22169°W; Top 51.30823°S, 72.19668°W.

TABLE 2 | Lithofacies codes, sedimentary structures, and interpretations used in this study (modified after Miall, 1978).

Lithofacies code	Description	Interpretation
Gt	Matrix-supported granule to cobble conglomerate, trough cross-stratification	Channel fill deposits
Gh	Clast-supported granule to cobble conglomerate, crudely or horizontally bedded, imbrication	Longitudinal bedforms, lag deposits, sieve deposits
St	Fine- to very coarse-grained pebbly sandstone, solitary or grouped trough cross-stratification	Sinuous crested or isolated dunes
Sp	Fine- to very coarse-grained pebbly sandstone, solitary or grouped planar cross-stratification	Straight crested dunes
Sh	Fine- to very coarse-grained pebbly sandstone, horizontal and ripple laminations	Plane-bed flow (critical flow)
Sl	Fine- to very coarse-grained pebbly sandstone, angle cross-stratification	Scour fills, humpback or washed-out dunes, antidunes
Fl	Fine sandstone, siltstone and mudstone, horizontal and ripple laminations	Overbank, abandoned channel or waning flood deposits
C	Coal, carbonaceous mud, plant debris, and mud films	Vegetated swamp deposits

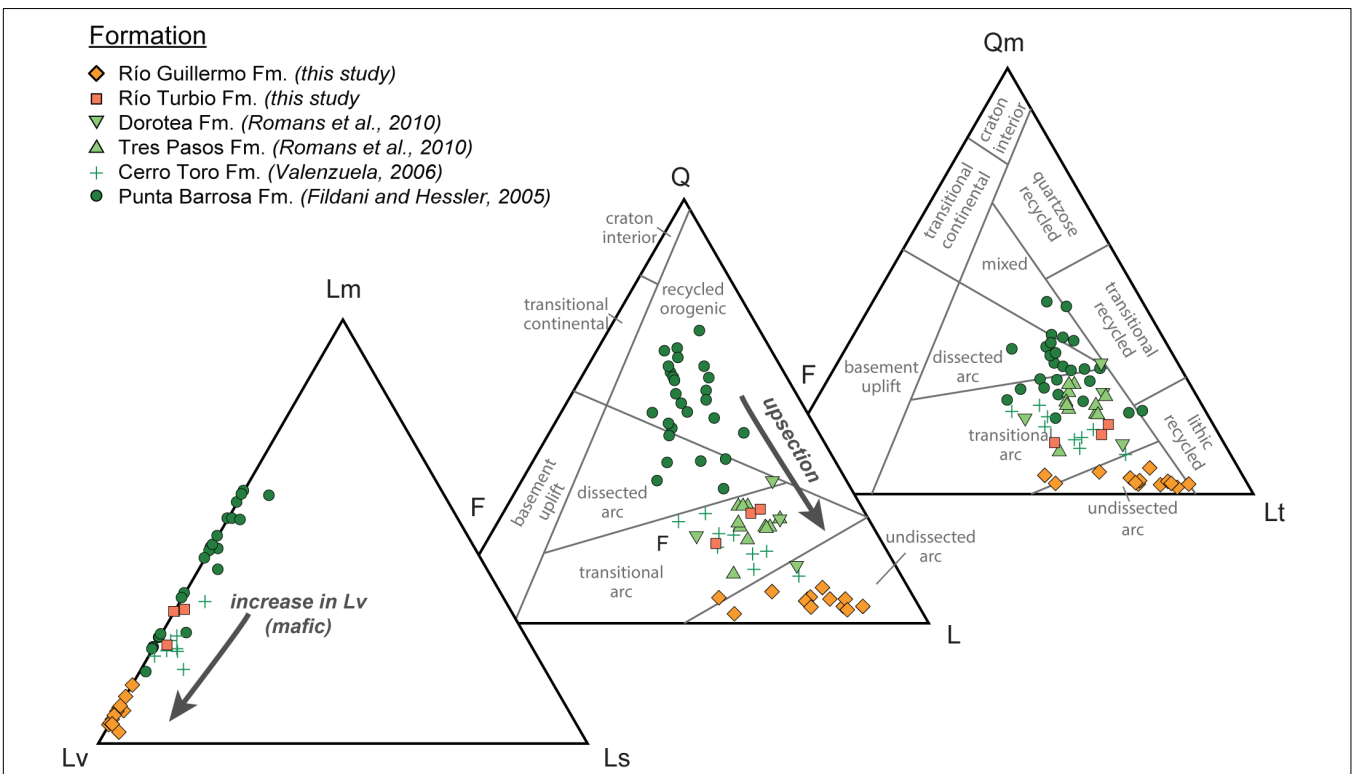

FIGURE 4 | Sandstone modal petrographic data from the Río Turbio Formation (red squares) and Río Guillermo Formation (orange diamonds) shown in comparison to published petrographic data from the Magallanes-Austral Basin. Refer to **Table 3** for parameters. Tectonic provenance fields are from Dickinson (1985). QFL (Quartz-Feldspar-Lithics) and QmFLt (Monocrystalline quartz-Feldspar-Lithic total) data show an upsection trend of decreasing in compositional maturity toward *undissected arc* source areas. LmLvLs data show a shift from Lm toward Lv, suggesting that the influx of mafic volcanic arc sediment is swamping any other recycled orogenic sources. Published datasets from the Upper Cretaceous basin infill are compiled from Fildani and Hessler (2005), Valenzuela (2006), and Romans et al. (2010).

conglomerate beds consisted of sufficiently large clasts (coarse pebbles and small cobbles) to allow for petrological identification in the field. To minimize bias toward more durable clast types, we used the area counting technique (Howard, 1993) for all pebble- and cobble-sized clasts until 60 counts were reached for four of five stations, while the stratigraphically highest count was limited by the fine grain-size. We report normalized compositions from seven diagnostic clast lithologic compositions: pale green metavolcanic, white quartz, mafic volcanic, mudstone, dark schist, granitoid, and intermediate-felsic volcanic (**Figure 5D**). Recalculated data are shown in **Table 4**.

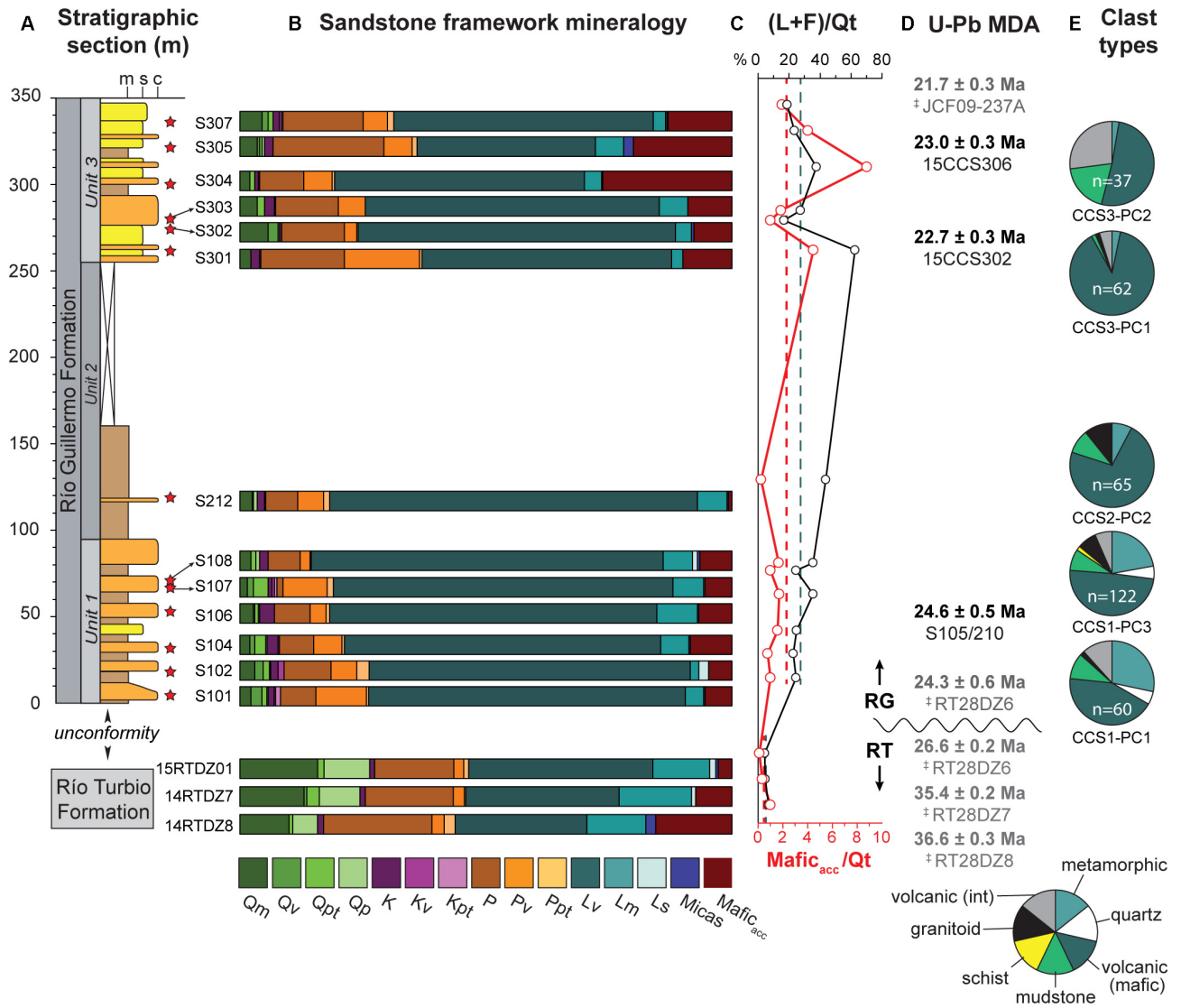

FIGURE 5 | Summary of modal sandstone petrography, clast compositions, and MDA from the Río Guillermo Formation at Cancha Carrera. Data from the underlying upper Río Turbio Formation are shown for comparison (stratigraphic positions approximated). **(A)** Simplified stratigraphic column. **(B)** Sandstone framework mineralogy. See **Table 4** caption for mineralogic abbreviations and section "Upper Oligocene-Lower Miocene Tectonics and Sedimentation History" for detailed discussion of trends. **(C)** (L + F)/Qt and $Mafic_{acc}$/Qt plots show relative immaturity (in %) of Río Guillermo Formation vs. upper Río Turbio Formation Dashed line represents the average of data for respective formations. **(D)** Relative contributions of clasts shown approximately in stratigraphic position – see **Figure 3** for sample locations. **(E)** Maximum depositional ages (MDA) interpreted from detrital zircon U-Pb geochronology. For comparison, ‡ denotes samples from Fosdick et al. (2019).

Conglomerate compositions throughout the Río Guillermo Formation are dominated (up to ∼90%) by mafic volcanic clasts (**Figure 5E**). There is an upsection decrease in pale green metavolcanic clasts and white quartz pebbles; we do not find white quartz pebbles in the upper part of the section (Units 2 and 3). Intermediate-felsic volcanic clasts are abundant at the base and top of the section. Granitoid clasts steadily increase in relative abundance through the lower part of the section, but become sparse upsection. Persistent, but subordinate, amounts of mudstone are also present, and rare biotite schist clasts were found in the bottom of the section.

Detrital Zircon U-Pb LA-ICP-MS Geochronology

Standard 5–6 kg samples were collected at regular intervals within the Río Guillermo Formation (**Figure 3** and **Table 1**). Mineral separations were performed by ZirChron, LLC using standard crushing, grinding, density, and heavy liquid procedures. Samples from the lower Río Guillermo Formation yielded very few zircon, and samples collected higher in the section were only modestly more zircon fertile. We re-processed our mineral concentrates to capture all available zircon; however, the zircon yield was limited by the sample volume. All extracted

TABLE 3 | Recalculated modal sandstone composition data.

Sample	Counts	Qm	Qv	Qpt	Qp	K	Kv	Kpt	P	Pv	Ppt	Lv	Lm	Ls	Micas	Mafic Acc.
	n	(%)	(%)	(%)	(%)	(%)	(%)	(%)	(%)	(%)	(%)	(%)	(%)	(%)	(%)	(%)
14RTDZ-8	400	10	0	0.8	5	1.3	0	0	22	2.5	2.3	26.8	12	0	2	15.5
14RTDZ-7	353	13	0.6	2.5	8.2	1.1	0	0	17.8	2.3	0.3	31.2	14.7	0.8	0	7.4
15RTDZ01	400	15.8	0	1.3	9.8	1	0	0	16	2	1	37.3	11.5	1.3	0.5	2.8
15CCS101	401	2.2	2.2	1	0.2	1.2	0.2	1	7.2	10.2	0.5	64.3	3.7	0	0.2	5.5
15CCS102	400	3	1.8	1.3	0.3	1.5	1.3	0	9.5	5.3	2.5	65.3	1.8	2	0	4.8
15CCS104	400	2	1	2.3	0.3	2.3	0.3	0	7	5.8	0.5	64.3	5.8	0	0.3	8.5
15CCS106	400	2.8	0.3	0.8	0.3	3	0	0	7.3	3.3	0.8	66.5	8.3	0	0.3	6.8
15CCS107	400	1.5	1.3	3	0	0.8	0.5	0.5	1.3	9	1.3	69	6.3	0.3	0	5.5
15CCS108	400	2.3	0	1	0.8	1.8	0	0	6.5	2	0.3	71.5	6	1	0.5	6.5
15CCS212	400	2.5	0	0.3	0.8	1.5	0.3	0	6.5	5.3	1.3	74.8	6	0	0.3	0.8
15CCS301	400	2.3	0	0	0	1.8	0.3	0	17	16.5	0.5	49.5	2.3	0	0	10
15CCS302	400	5.8	2	0	0.3	0.5	0	0	12.8	2.5	0.3	64.5	3.3	0	0.5	7.8
15CCS303	400	3.5	0	1.5	0	2	0.3	0	12.8	5.5	0	59.8	5.8	0	0	9
15CCS304	400	2	0	1	0	0.8	0.3	0	9	5.8	0.5	50.8	3.5	0	0.3	26.3
15CCS305	400	4.5	1.3	1	0	1.3	0.5	0.3	16.3	5	1.3	52.8	2.5	0.3	0.3	13
15CCS307	400	3.5	0.5	0.5	0.5	1.8	0	0	22.5	5.8	1	36.3	5.8	0	2	20

Qm, monocrystalline quartz; Qv, volcanic quartz; Qpt, plutonic quartz; Qp, polycrystalline quartz; K, mono-crystalline K-feldspar; Kv, volcanic K-feldspar; Kpt, plutonic K-feldspar; P, monocrystalline plagioclase feldspar; Pv, volcanic plagioclase feldspar; Ppt, plutonic plagioclase feldspar; Lv, volcanic lithic; Lm, metamorphic lithic; Ls, sedimentary lithic; Micas, Bt + Chl + Mu; Mafic$_{acc}$, Amphibole + Pyroxene (cpx) + Ol.

TABLE 4 | Recalculated modal clast composition data.

Count name	Clasts counted	Pale green metavolcanic	White quartz	Mafic volcanic	Mudstone	Schist (dark)	Granitoid	Intermediate volcanic
	(*n*)	(%)	(%)	(%)	(%)	(%)	(%)	(%)
CCS1-PC1	60	28.3	5	43.3	10	0	1.7	11.7
CCS1-PC3	122	22.1	4.9	49.2	8.2	1.6	7.4	6.6
CCS2-PC2	65	7.7	0	72.3	9.2	0	10.8	0
CCS3-PC1	62	3.2	0	88.7	1.6	0	1.6	4.8
CCS3-PC2	37	2.7	0	51.4	18.9	0	0	27

individual zircons from each sample were hand-picked and mounted on double-sided tape to make them available for future (U-Th)/He double dating. Zircon U-Pb LA-ICPMS analyses were conducted at University of Arizona LaserChron Center following analytical procedures of Gehrels (2012). Grains were analyzed at random to avoid bias in detrital age distributions. A very small percentage of grains have anomalously high analytical uncertainty (>20%, 1σ) in $^{207}Pb/^{235}U$ and were excluded from final age distributions. However, inclusion of these grains does not substantively affect any interpretations put forward. Given the low zircon yield of these samples, our data interpretations are largely summarized for the formation in general, rather than detailed upsection changes in age spectra. Maximum depositional ages (MDA) (**Table 1**) are calculated based on youngest age populations defined by three or more overlapping zircon ages (2σ). Refer to **Supplementary Table S3** for detrital zircon LA-ICPMS data.

Detrital zircon analyses from both the upper Río Turbio Formation and Río Guillermo Formation are characterized by bimodal distributions of Cenozoic and Cretaceous populations with very few Paleozoic and older grains (**Figure 6**). Cretaceous ages from both formations are characterized by bimodal distributions; however, the youngest of these modes (67–78 Ma) is a new association that does not correspond with known bedrock geochronology (Hervé et al., 2007). A prominent Eocene peak (30–40 Ma) is an exclusive feature of the upper Río Turbio Formation, while Neogene ages characterize Cenozoic populations in the Río Guillermo Formation This Eocene peak is also a new association and post-dates known Paleogene magmatism in the Southern Patagonian Batholith (Hervé et al., 2007).

Sample 15CCS105/210 is a composite from stratigraphically adjacent locations in the lower part of the section, both with poor zircon yields, 24 and 57 grains, respectively. Ages range from *ca.* 24 to 503 Ma, with a single significant Cenozoic peak centered at *ca.* 25 Ma populated by the 10 youngest grains, a broadly bimodal Cretaceous age group with peaks at (74, 79, and 83 Ma) defining the younger mode and (100, 105, and 108 Ma) defining the older mode, and a minor Late Jurassic age peak. An error-weighted mean of the youngest coherent zircon population ($n = 7$) yields a calculated MDA of 24.6 ± 0.5 Ma (2σ). This age overlaps with the calculated MDA of 24.3 ± 0.6 Ma (2σ) from the stratigraphically

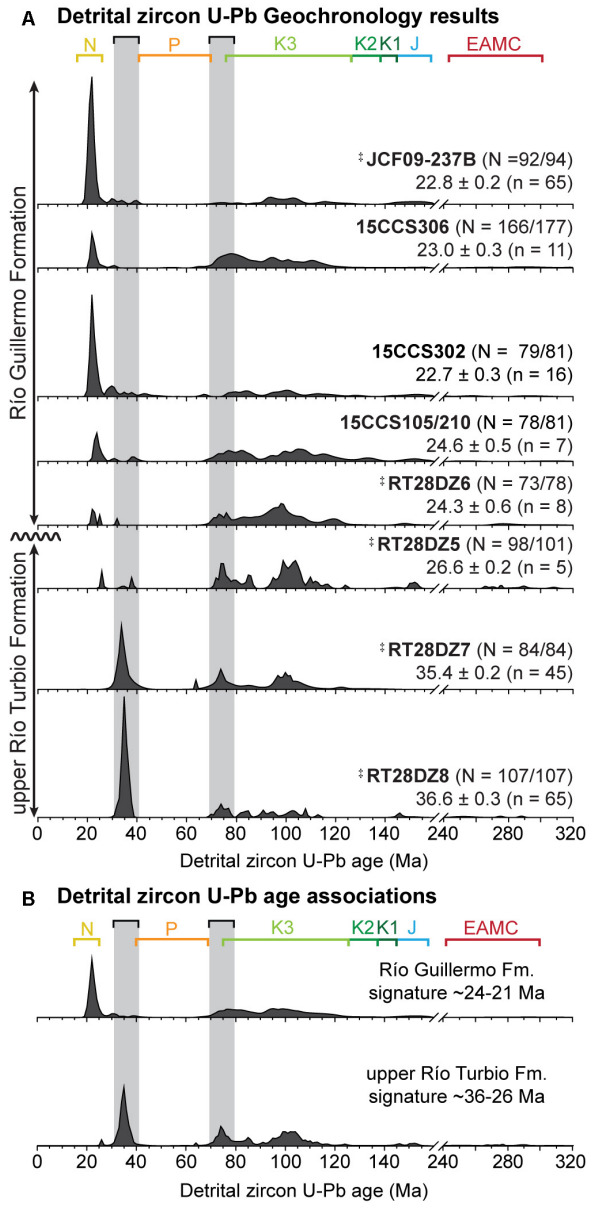

FIGURE 6 | Detrital zircon U-Pb LA-ICP-MS data showing upsection changes in provenance. **(A)** Normalized probability age distributions from the Río Guillermo and upper Río Turbio formations. Note the change in scale at 160 Ma. Ages of igneous sources as reported from Hervé et al. (2007) are Neogene (N), Paleogene (P), Cretaceous I (K1), Cretaceous II (K2), and Cretaceous III (K3), Jurassic (J), and Eastern Andean Metamorphic Complex (EAMC). **(B)** Combined detrital zircon age associations for the pre-tectonic and post-tectonic sediment sources, showing a loss of a predominant 30–40 Ma source prior to 24 Ma. ‡ denotes samples from Fosdick et al. (2019).

lower RT28DZ6 from Fosdick et al. (2019) at the base of the Río Guillermo Formation, which does not suffer from similarly low zircon fertility.

Sample 15CCS302 had a relatively higher zircon yield of 108 grains but contained a significant number of grains excluded due to high (>20%) analytical uncertainty. The age distribution is characterized by a strong *ca.* 23 Ma peak populated by the 33 youngest grains, a minor Eocene peak at 32 Ma, and minor Late and middle Cretaceous modes defined by peaks at 81, 85, and 101 Ma, respectively. An error-weighted mean of the youngest coherent zircon population (n = 16) yields a calculated MDA of 22.7 ± 0.3 Ma (2σ).

Sample 15CCS306 had a moderate zircon yield producing 198 grains, with 177 of those analyses within threshold uncertainty. Age distributions show a well-defined *ca.* 23 Ma early Miocene peak, and significant Late – Early Cretaceous age groups with peaks at (75, 79, 89, 96, and 106 Ma). An error-weighted mean of the youngest coherent zircon population (n = 11) yields a calculated MDA of 23.0 ± 0.3 Ma (2σ).

DISCUSSION

Integrated sedimentary provenance and sedimentology from the Río Guillermo Formation capture the drainage configuration during latest Oligocene – early Miocene development of the southern Patagonian Andes. Here, we discuss the detailed provenance signatures within the context of the kinematic history of the Patagonian fold-and-thrust belt and the long-term foreland basin record. Specifically, this synthesis explores the regional driving factors and chronologic progression of the structural and topographic development of an orogenic wedge during forced adjustment to incorporation of inherited basin structures (Fosdick et al., 2011) and migration of the locus of exhumation (Thomson et al., 2001; Fosdick et al., 2013).

Interpreted Provenance of the Upper Oligocene – Lower Miocene Basin Fill

We interpret the collective provenance datasets of modal sandstone, conglomerate compositions, and detrital zircon geochronology across the transition from proximal upper Oligocene to middle Miocene deposits preserved in the basin at this latitude. Below we outline distinct provenance trends observed within the upper Río Turbio Formation and overlying Río Guillermo Formation that support (1) a shift from transitional to undissected arc source areas, (2) persistent connectivity to the syndepositional volcanic arc, (3) waning sediment contribution from internal fold-thrust belt (Jurassic and Paleozoic), and (4) a pronounced loss of the late Eocene (~40–30 Ma) zircon source areas in earliest Oligocene time.

Sandstone provenance of the upper Río Turbio Formation is consistent with a *transitional arc* source (c.f. Dickinson, 1985), and has similar compositional character to the underlying Dorotea, Tres Pasos, and Cerro Toro formations of the external fold-and-thrust belt (**Figures 1B**, **4**). We interpret this consistency to suggest either (1) a stable source area despite substantial unconformities, changes in sedimentation style, and depositional environments contained within that stratigraphic succession during this time interval, and/or (2) recycling of these underlying units where they are exposed in thrust sheet hanging-wall blocks to the west of our study area (**Figure 1**). Locally, upsection trends within the upper Río Turbio Formation include

a progressive loss of labile minerals (i.e., amphibole, pyroxene, olivine) and increase in quartz grains (**Figure 5B**), which could be due to winnowing effects during recycling and higher rates of weathering in the source areas (e.g., Johnsson, 1993; Cox et al., 1995). The Upper Cretaceous basin infill, and in particular the Punta Barrosa Formation, contains abundant metamorphic lithics representative of the EAMC and hinterland thrust domain (**Figure 4**). Therefore, within the upper Río Turbio Formation, the maturation of sandstone compositions and comparable or lesser relative abundance of L_m lithics may record recycled provenance from these external fold-and-thrust belt sources. The lack of Paleocene zircons precludes the underlying Cerro Dorotea Formation (Fosdick et al., 2019) as a source, suggesting these strata were not yet exposed during deposition of the Río Turbio and Río Guillermo formations.

Provenance data from the overlying Río Guillermo Formation suggest a distinct shift in the sediment source areas to a mafic volcanic arc, and lesser contributions from the hinterland thrust domain or external fold-and-thrust belt (**Figures 4**, **5B,C,E**). Sandstones are texturally and compositionally extremely immature throughout, as evidenced by high relative abundance of volcanic lithic grains and mafic minerals, and dearth of quartz (**Figure 4**). These data also preclude any significant recycling from Río Turbio Formation equivalent or older foreland basin strata as a significant potential sediment source. Rather, the abundance of chemically and physically susceptible sandstone grains (e.g., volcanic lithics and mafic minerals and/or those dominant cleavage planes) is consistent with direct sourcing from the active magmatic arc. Whole rock $^{40}Ar/^{39}Ar$ ages and major and trace element geochemistry from the mafic volcanic clasts indicate Miocene (25–22 Ma) eruptive ages with arc geochemistry (VanderLeest et al., 2018). The prominent Miocene zircon U-Pb age peak generally youngs upsection within the Río Guillermo Formation and supports direct connectivity with the magmatic arc (**Figure 6**).

Maintenance of a direct sediment routing pathway from the magmatic arc to the proximal foredeep through Oligocene-Miocene sedimentation is supported by younging of youngest detrital age populations from ∼33 Ma to ∼21 Ma upsection (**Figure 6A**). We note, however, the abrupt loss of the prominent Eocene zircon U-Pb age peak (40–30 Ma) at the top of the upper Río Turbio Formation (between samples RT28DZ7 and RT28DZ5; **Figure 6A**). This Eocene peak is not a previously recognized phase of arc magmatism identified within the SPB or associated volcanic rocks (Hervé et al., 2007), suggesting limited original extent of Eocene magmatism and/or underrepresentative sampling due to remote access of the fjords. The loss of the Eocene arc source during Río Guillermo deposition may be interpreted as either isolation of the Eocene source by Oligocene-Miocene volcanic cover or intervening thrust sheets, or erosional removal. The "reappearance" of the Eocene age peak in younger overlying strata may indicate recycling of Paleogene deposits (Fosdick et al., 2015), or drainage reorganization with directly sourced remnants of the Eocene arc.

In addition to the syndepositional volcanic arc primary source area to the Río Guillermo Formation, we evaluate direct or recycled sediment sources from other orogenic source areas. Evidence of subordinate sediment contribution from the hinterland thrust domain or external fold-and-thrust belt include the pale green metavolcanic and white quartz clasts (∼20%), diagnostic of the Upper Jurassic Tobífera Formation, and biotite schist clasts (<5%) that are likely derived from EAMC basement rocks (**Figure 5E**). Additionally, well-indurated extrabasinal mudstone clasts (6–18%), which are least diagnostic in terms of potential source areas, but point to either the hinterland thrust domain and/or external fold-and-thrust belt source areas (e.g., Zapata Formation and/or mudstone-rich facies of the Cerro Toro Formation). These sediment types are challenging to interpret because they could be derived directly from the hinterland thrust domain (**Figure 1**), or recycled from the external fold-and-thrust belt, which includes similar hinterland and batholith derived provenance signatures. Specifically, SPB-derived granitoid clasts and metarhyolite clasts from the Tobífera Formation are abundant in the Cenomanian Cerro Toro Formation (Crane, 2004; Valenzuela, 2006), which comprises part of the external fold-and-thrust belt. The Late Cretaceous detrital zircon U-Pb age clusters reflect either direct sourcing from the eroded batholith or recycled zircons from the external fold-and-thrust belt (e.g., Romans et al., 2010; Fosdick et al., 2015). The decrease in relative abundance of metarhyolite clasts and substantial lack of Late Jurassic zircon U-Pb ages may indicate dilution of the Tobífera Formation clasts as the syndepositional arc source areas became dominant.

Due to the paucity of Jurassic and Paleozoic U-Pb zircon ages or sediment types (metamorphic lithics, SPB granitoids) characteristic of the hinterland thrust domain, we prefer an interpretation for the Río Guillermo Formation as (1) direct sourcing of the active Miocene arc, with (2) lesser recycled sediment input from the external fold-thrust-belt. In this scenario, the headwaters of the ancestral Río Guillermo resided in the extensive Miocene volcanic highlands, but the drainage network largely bypassed the hinterland thrust domain. This scenario may be analogous to the changes in basin configuration interpreted for the Neogene Bermejo Basin in the Central Andes, where uplift of the Precordillera caused river drainage reorganization that shifted from a mixture of Precordillera and hinterland-derived source areas, to a regional point-source within the hinterland Frontal Cordillera (Jordan et al., 1993).

Upper Oligocene-Lower Miocene Tectonics and Sedimentation History

Our new provenance interpretations from the upper Oligocene through lower Miocene Magallanes-Austral Basin at Estancia Cancha Carrera indicate a major shift in source areas that is consistent with rejuvenation of arc magmatism and a tectonic reorganization of the hinterland and fold-and-thrust belt. This shift in sedimentary provenance between ∼27 and 24 Ma that predates a basin margin change in depositional environment and transition from shallow marine to fluvial sedimentation, as recorded by the Río Guillermo Formation. Here, we compare the timing of eustatic sea level variations, retroarc deformation, and plate convergence rates, to understand the geologic context

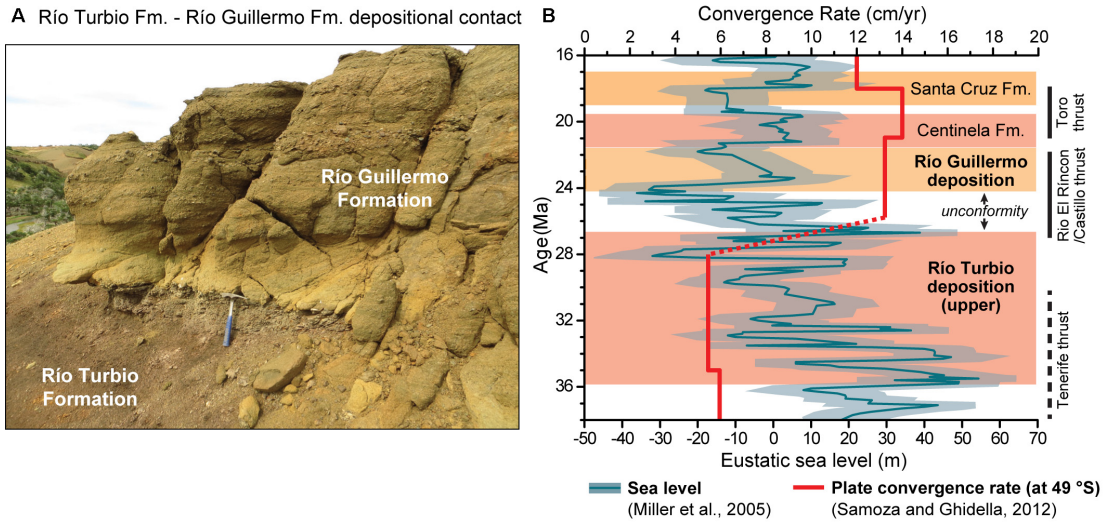

FIGURE 7 | (A) Outcrop photograph of the disconformable contact between the Río Guillermo Formation and underlying upper Río Turbio Formation at the Cancha Carrera study locality. **(B)** Changes in eustatic sea level during deposition of the foreland basin deposits in our study area. Sea level data from Miller et al. (2005). Convergence rates between the South America and Farallon plates for 49°S from Somoza and Ghidella (2012). Timing of faulting in the external fold-and-thrust belt from Fosdick et al. (2011). Depositional ages from Fosdick et al. (2015, 2019), and references therein. The erosional unconformity between the Río Turbio and Río Guillermo formations corresponds in time and duration to a long-term drop in eustatic sea level.

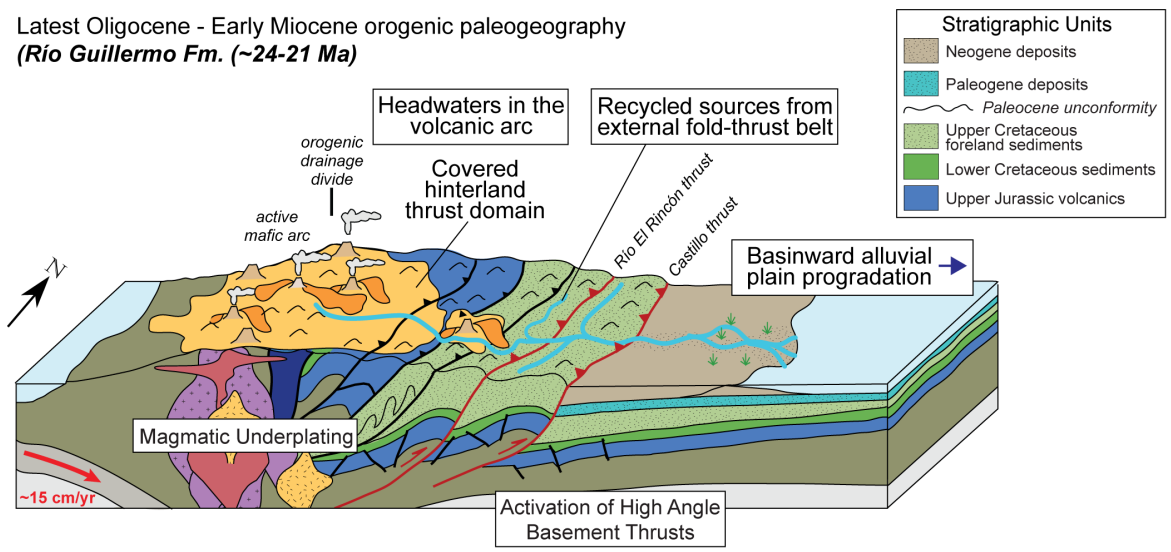

FIGURE 8 | Schematic paleogeographic cartoon of the late Oligocene – early Miocene orogenic configuration during deposition of the Río Guillermo Formation. Modified from Fosdick et al. (2015) with new learnings specifically to this time interval.

for these changes in sediment source areas in Patagonia, with implications for orogenic and basin sedimentation processes.

The ~2 Myr disconformable contact between the uppermost Río Turbio Formation and Río Guillermo Formation reflects a change from marginal marine to fluvial depositional environments (**Figure 7A**) that we suggest is at least partially influenced by a global regression across this time interval. By ~24 Ma, eastward directed fluvial sedimentation was established, representing a basin margin shallowing to non-marine conditions. Sedimentation of the entire ~350 m compacted thickness of the Río Guillermo Formation at Estancia Cancha Carrera is tightly constrained to ~2.5 Myr. This requires sufficient basin accommodation and sediment flux to produce a modest sedimentation rate (~0.14 km/Myr) over this time interval, on par with Neogene rates observed elsewhere in the Andean foreland basin systems (e.g., Goddard and Carrapa, 2018). Over that corresponding time interval, eustatic sea level is characterized by an abrupt 30–50 m rise and relative highstand (Miller et al., 2005; **Figure 7B**). This transgression is well-recorded in the more distal reaches of the basin, as recorded

in coeval shallow marine deposits of the San Julián Formation along the present-day Atlantic coast (Parras et al., 2008, 2012).

The kinematic development of the Patagonian fold-and-thrust belt records a decrease in upper crustal shortening since Late Cretaceous time, along with a deepening of the basal detachment in at least two stages of Cenozoic deformation (Fosdick et al., 2011). Based on structural mapping, seismic-reflection data, cross-cutting relationships, and available chronology of synorogenic foreland basin deposits, Fosdick et al. (2011) documented two phases of Cenozoic deformation characterized by basement-involved shortening and deepening of the decollement: Stage IV (∼27–21 Ma), with faulting of the Río Rincon and Castillo faults along a reconstructed decollement depth of ∼8–10 km; and Stage V (∼21–18 Ma), with further deepening of the decollement to ∼16–18 km along the Toro thrust. The little crustal shortening represented by these deformational phases (∼3–4 km) are consistent with high-angle fault geometries, several km of vertical rock uplift, and regional exhumation across the external fold-and-thrust belt (Fosdick et al., 2011, 2013). Both basement faulting stages are interpreted as inverted Mesozoic normal faults based on outcrop and subsurface data. Revised chronology of the Cenozoic foreland basin deposits (Fosdick et al., 2019), specifically the uppermost upper Río Turbio Formation (∼26 Ma) and Río Guillermo Formation (∼24–21 Ma), correspond in time to Stage IV, and perhaps the earliest part of Stage V. Our provenance interpretations from these deposits record a shift from *transitional arc* to *undissected arc* sources by between ∼27 and ∼24 Ma that was coeval with the widening of the orogenic wedge via forward propagation of reactivated basement faulting during Stage IV faulting (**Figure 8**).

Within the upper Río Turbio Formation, the maturation of sandstone compositions and persistent presence of L_m and L_s lithics may record continued sourcing from the hinterland prior to the major shift toward volcanic highland topography by 24 Ma. Starting ∼24 Ma at the base of Río Guillermo Formation, generation of volcanic highland topography due to rejuvenated magmatic arc provided volcanic sediment to the foreland basin margin (**Figure 8**). The relative paucity of sediment derived directly from the hinterland thrust domain may be explained by trunk rivers connected to the upland and arc, thereby routing around the retroarc foreland topography (**Figure 8**).

Previous workers have linked the Stage IV Río El Rincón-Castillo faulting to more rapid and orthogonal plate convergence between the Nazca and South American plates (Fosdick et al., 2013) and potential increase in retroforeland convergence due to transpressive development of the North Scotia Ridge (Bry et al., 2004; Lagabrielle et al., 2009; Fosdick et al., 2011). As the thrust front migrated cratonward, deformation along the Río El Rincón-Castillo faults (**Figure 8**) may have been localized by pre-existing basement structures beneath the foreland (Fosdick et al., 2011). Re-activation of these basement structures may have had the effect of changing the stress state of the orogenic wedge by activating a deeper sole-out depth (e.g., Hilley et al., 2005) and promoting vertical topographic uplift across the external fold-and-thrust belt. We posit that, although this phase of deformation caused foreland basin subsidence and sedimentation of the lower Miocene Río Guillermo Formation, headwaters located within the volcanic highlands, rather than the thrust sheets, provided the primary sediment flux to the basin margin (**Figure 8**).

The rejuvenation of the Miocene volcanic arc is consistent with an acceleration in plate convergence rates that occurred between 28 and 25 Ma prior to the breakup of the Farallon plate (Somoza and Ghidella, 2012; **Figure 7B**), which may have driven enhanced hydration melting and retroarc deformation. This scenario is consistent both with the uptick in early Miocene arc volcanism (VanderLeest et al., 2018) and provenance data reported here. Although this episode of orogenesis in Patagonia was limited in the magnitude of deformation and basin subsidence compared to elsewhere along the Andes (e.g., see Horton, 2018 for a recent synthesis), our data characterize the orogen-to-basin connection during this brief phase of retroarc deformation in Patagonia.

Lastly, the thermochronologic record from the Patagonian Andes suggests a post late Oligocene eastward migration of the locus of maximum denudation that we discuss briefly within the context of the Río Guillermo foreland basin history. Apatite fission track cooling ages from the Southern Patagonian Batholith document accelerated cooling and inferred denudation from ∼30 to 23 Ma (Thomson et al., 2001). Subsequently, this locus of maximum denudation shifted to the eastern margin of the batholith (**Figure 1**) until ∼18–14 Ma, which has been interpreted as an eastward migration in the topographic crest during that time (Thomson et al., 2001). Thus, the locus of maximum denudation during Río Guillermo deposition would have likely corresponded to the Miocene volcanic arc highlands (since eroded away) constructed within the Mesozoic batholith (**Figure 8**). We interpret the lack of substantial thrust belt provenance in the Río Guillermo Formation to be explained by a point-source routing system in the volcanic arc. Farther east, thermal history modeling of zircon (U-Th)/He thermochronology data suggest focused denudation between ∼17 and 16 Ma within the external fold-and-thrust belt, suggesting exhumation of at least 5 km since that time (Fosdick et al., 2013; Goddard and Fosdick, 2019). This sediment sourced from the more recently, deeply exhumed external-fold-and-thrust belt was likely shed into the offshore basins (Ghiglione et al., 2016), possibly in response to subduction of the Chile Ridge spreading ridge (Goddard and Fosdick, 2019).

CONCLUSION

Integration of sedimentary provenance analysis from the uppermost Río Turbio and Río Guillermo formations highlight the abrupt transition between ∼27 and 24 Ma from dissected/transitional arc to undissected arc that represents erosion of the mafic volcanic highlands. The Oligocene upper Río Turbio Formation likely records early uplift and erosion of the proximal Río El Rincón-Castillo thrusts of the external fold-and-thrust belt, prior to rejuvenated arc activity. Between

∼24 and 21 Ma deposition of the Río Guillermo Formation, the active arc provided most of the sediment supply to the retroarc foreland basin, despite coeval changes in orogenic wedge dynamics and uplift and exhumation of the intervening external-fold-and-thrust belt along a deeper detachment and reactivation of high-angle basin structures (**Figure 8**). These structures originated as high-angle normal faults related to the predecessor Rocas Verdes Basin extensional history that were reactivated during advancement of the foreland deformational front. This provenance record provides additional context for inferred migrations of the paleotopographic crest and magmatic arc based on low-temperature thermochronology datasets. These findings have important implications for interpreting paleogeographic changes and tectonic signals from provenance data in retroarc settings dominated by volcanic sources (Varela et al., 2013), where sustained arc activity may overwhelm the signal of late-stage deformation. In the case of the Magallanes-Austral Basin, the Río Guillermo Formation tracks one of the final phases of Cordilleran orogenesis prior to plate reorganization and subduction of the impinging Chile Ridge spreading center.

DATA AVAILABILITY STATEMENT

All datasets generated for this study are included in the article/**Supplementary Material**.

AUTHOR CONTRIBUTIONS

JL and JF participated in project fieldwork, collection of clast count and stratigraphic data, and sampling for geochronology and sandstone petrography. JL performed zircon LA-ICPMS geochronology, sandstone petrographic analyses, and preliminary interpretations. JL, JF, and RV contributed to data synthesis, interpretations, and manuscript preparation. JF developed the project idea and secured financial support.

FUNDING

This research was supported by the U.S. National Science Foundation Award EAR-1649585 to JF, the Robert R. Shrock Foundation at Indiana University, and the Geological Society of America Graduate Research Grant Program.

ACKNOWLEDGMENTS

We acknowledge B. Romans, T. Schwartz, E. Bostelmann, R. Ugalde, M. Griffin, A. Parras, M. Ghiglione, and M. Hren for insightful discussions on Patagonian geology. J. L. Oyarzún and N. Raffer graciously provided logistical support. We thank S. F. Alvarez for permission to conduct fieldwork at the Estancia Cancha Carrera. The Arizona LaserChron Center (NSF Award EAR-1338583) provided expert analytical assistance. Reviews by EF, BH, JS, and editor DH greatly improved the scope and clarity of this manuscript.

SUPPLEMENTARY MATERIAL

The Supplementary Material for this article can be found online at: https://www.frontiersin.org/articles/10.3389/feart.2019.00353/full#supplementary-material

REFERENCES

Allen, P. A., and Heller, P. L. (2011). "Dispersal and preservation of tectonically generated alluvial gravels in sedimentary basins," in *Tectonics of Sedimentary Basins: Recent Advances*, eds C. Busby, and A. Azor, (Oxford, UK: Blackwell Publishing Ltd.), 111–130. doi: 10.1002/9781444347166.ch6

Armitage, J. J., Duller, R. A., Whittaker, A. C., and Allen, P. A. (2011). Transformation of tectonic and climatic signals from source to sedimentary archive. *Nat. Geosci.* 4, 231–235. doi: 10.1038/NGEO1087

Biddle, K. T., Uliana, M. A., Mitchum, R. M., Fitzgerald, M. G., and Wright, R. C. (1986). "The stratigraphic and structural evolution of the central and eastern Magallanes Basin, southern South America," in *Foreland Basins*, eds P. A. Allen, and P. Homewood, (Oxford, UK: Blackwell Publishing), 41–61. doi: 10.1002/9781444303810.ch2

Blisniuk, P. M., Stern, L. A., Chamberlain, C. P., Idleman, B., and Zeitler, P. K. (2005). Climatic and evologic changes during Miocene surface uplift in the Southern Patagonian Andes. *Earth Planet. Sci. Lett.* 230, 125–142. doi: 10.1016/j.epsl.2004.11.015

Breitsprecher, K., and Thorkelson, D. J. (2009). Neogene kinematic history of Nazca-Antarctic-Phoenix slab windows beneath Patagonia and the Antarctic Peninsula. *Tectonophysics* 464, 10–20. doi: 10.1016/j.tecto.2008.02.013

Bry, M., White, N., Singh, S., England, R., and Trowell, C. (2004). Anatomy and formation of oblique continental collision: South Falkland basin. *Tectonics* 23, 1–20. doi: 10.1029/2002TC001482

Burbank, D. W., Beck, R. A., Raynolds, R. G. H., Hobbs, R., and Tahirkheli, R. A. K. (1988). Thrusting and gravel progradation in foreland basins: a test of post-thrusting gravel dispersal. *Geology* 16, 1143–1146.

Calderón, M., Fosdick, J. C., Warren, C., Massonne, H.-J., Fanning, C. M., Fadel Cury, L., et al. (2012). The low-grade Canal de las Montañas Shear Zone and its role on the tectonic emplacement of the sarmiento ophiolitic complex and late cretaceous Patagonian Andes orogeny, Chile. *Tectonophysics* 524, 165–185. doi: 10.1016/j.tecto.2011.12.034

Calderón, M., Hervé, F., Fuentes, F., and Fosdick, J. C. (2016). "Tectonic evolution of Paleozoic and mesozoic andean metamorphic complexes and the Rocas Verdes ophiolites in southern Patagonia," in *Geodynamic Evolution of the Southernmost Andes*, ed. M. Ghiglione, (Berlin: Springer-Verlag), 7–36. doi: 10.1007/978-3-319-39727-6_2

Cande, S. C., and Leslie, R. B. (1986). Late Cenozoic tectonics of the Southern Chile trench. *J. Geophys. Res. Solid Earth* 91, 471–496.

Cox, R., Lowe, D. R., and Cullers, R. L. (1995). The influence of sediment recycling and basement composition on evolution of mudrock chemistry in the southwestern United States. *Geochim. Cosmochim. Acta* 59, 2919–2940. doi: 10.1016/0016-7037(95)00185-9

Crane, W. H. (2004). *Depositional History of the Upper Cretaceous Cerro Toro Formation, Silla Syncline, Magallanes Basin, Chile*. Ph.D. thesis, Stanford University, Stanford, CA.

Cunningham, W. D., Dalziel, I. W. D., Lee, T.-Y., and Lawver, L. A. (1995). Southernmost South America-Antarctic Peninsula relative plate motions since 84 Ma: implications for the tectonic evolution of the Scotia Arc region. *J. Geophys. Res.* 100, 8257–8266. doi: 10.1029/95jb00033

Dahlen, F. A. (1984). Noncohesive critical Coulomb wedges: an exact solution. *J. Geophys. Res.* 89, 10125–10133. doi: 10.1029/jb089ib12p10125

Dalziel, I. W. D., de Wit, M. J., and Palmer, K. F. (1974). Fossil marginal basin in the southern Andes. *Nature* 250, 291–294. doi: 10.1038/250291a0

Daniels, B. G., Auchter, N. C., Hubbard, S. M., Romans, B. W., Matthews, W. A., and Stright, L. (2017). Timing of deep-water slope evolution constrained by large-n detrital and volcanic ash zircon geochronology, Cretaceous Magallanes Basin, Chile. *Bull. Geol. Soc. Am.* 130, 438–454. doi: 10.1130/B31757.1

Davis, D., Suppe, J., and Dahlen, F. A. (1983). Mechanics of fold-and-thrust belts and accretionary wedges. *J. Geophys. Res.* 88, 1153–1172.

de Wit, M. J., and Stern, C. R. (1981). Variations in the degree of crustal extension during formation of a back-arc basin. *Tectonophysics* 72, 229–260. doi: 10.1016/0040-1951(81)90240-7

DeCelles, P. G., and Mitra, G. (1995). History of the Sevier orogenic wedge in terms of critical taper models, northeast Utah and southwest Wyoming. *Geol. Soc. Am. Bull.* 107, 454–462. doi: 10.1130/0016-76061995107<0454

Dickinson, W. R. (1985). "Provenance relations from detrital modes of sandstones," in *Provenance of Arenites, NATO Advanced Science Institutes Series*, ed. G. G. Zuffa, (Washington, D.C: NATO), 333–362.

Dickinson, W. R., and Suczek, C. A. (1979). Plate tectonics and sandstone compositions. *Am. Assoc. Petrol. Geol. Bull.* 63, 2164–2182.

Eagles, G., and Jokat, W. (2014). Tectonic reconstructions for paleobathymetry in Drake Passage. *Tectonophysics* 611, 28–50. doi: 10.1016/j.tecto.2013.11.021

Fildani, A., and Hessler, A. M. (2005). Stratigraphic record across a retroarc basin inversion: rocas verdes–magallanes Basin, Patagonian Andes, Chile. *Geol. Soc. Am. Bull.* 117, 1596–1614. doi: 10.1130/B25708.1

Fildani, A., Romans, B. W., Fosdick, J. C., Crane, W. H., and Hubbard, S. M. (2008). "Orogenesis of the Patagonian Andes as reflected by basin evolution in southernmost South America," in *Ores and Orogenesis: Circum-Pacific Tectonics, Geologic Evolution, and Ore Deposits*, eds J. E. Spencer, and S. R. Titley, (Tucson: Arizona Geological Society), 259–268.

Fosdick, J., VanderLeest, R., Bostelmann, E., Leonard, J., Ugalde, R., Oyarzún, J., et al. (2019). Revised timing of Cenozoic Atlantic incursions and changing hinterland sediment sources during southern Patagonian orogenesis. *EarthArXiv* [Preprint]. doi: 10.31223/osf.io/vqkds

Fosdick, J. C., Grove, M. J., Graham, S. A., Hourigan, J. K., Lovera, O., and Romans, B. W. (2015). Detrital thermochonologic record of burial heating and sediment recycling in the Magallanes foreland basin, Patagonian Andes. *Basin Res.* 27, 546–572. doi: 10.111/bre.12088

Fosdick, J. C., Grove, M. J., Hourigan, J. K., and Calderón, M. L. (2013). Retroarc deformation and exhumation near the end of the Andes, southern Patagonia. *Earth Planet. Sci. Lett.* 361, 504–517. doi: 10.1016/j.epsl.2012.12.007

Fosdick, J. C., Romans, B. W., Fildani, A., Bernhardt, A., Calderón, M., and Graham, S. A. (2011). Kinematic evolution of the Patagonian retroarc fold-and-thrust belt and Magallanes foreland basin, Chile and Argentina, 51°30'S. *Geol. Soc. Am. Bull.* 123, 1679–1698. doi: 10.1130/B30242.1

Garcia-Castellanos, D., Fernandez, M., and Torne, M. (2002). Modeling the evolution of the Guadalquivir foreland basin (southern Spain). *Tectonics* 21, 9.1–9.17. doi: 10.1029/2001TC001339

Gehrels, G. (2012). "Detrital Zircon U-Pb geochronology: current methods and new opportunities," in *Tectonics of Sedimentary Basins: Recent Advances*, eds C. Busby, and A. Azor, (Oxford, UK: Blackwell Publishing Ltd.), 45–62. doi: 10.1002/9781444347166.ch2

George, S. W. M., Davis, S. N., Fernández, R. A., Manríquez, L. M. E., Leppe, M. A., Horton, B. K., et al. (2019). Chronology of deposition and unconformity development across the cretaceous–paleogene boundary, Magallanes-Austral Basin, Patagonian Andes. *J. South Am. Earth Sci.* 97:102237. doi: 10.1016/j.jsames.2019.102237

Ghiglione, M. C., Quinteros, J., Yagupsky, D., Bonillo-Martínez, P., Hlebzevtich, J., Ramos, V. A., et al. (2010). Structure and tectonic history of the foreland basins of southernmost South America. *J. South Am. Earth Sci.* 29, 262–277. doi: 10.1016/j.jsames.2009.07.2006

Ghiglione, M. C., Ramos, V., Cuitiño, J., and Barberón, V. (2016). "Growth of the Southern Patagonian Andes (46-53°S) and its relation with subduction processes," in *Growth of the Southern Andes*, eds A. Folguera, M. Naipauer, L. Sagripanty, M. C. Ghiglione, D. Orts, and L. B. Giambiagi, (Berlin: Springer), 201–240. doi: 10.1007/978-3-319-23060-3_10

Goddard, A. L. S., and Fosdick, J. C. (2019). Multichronometer thermochronologic modeling of migrating spreading ridge subduction in southern Patagonia. *Geology* 47, 555–558. doi: 10.1130/G46091.1/4678798/g46091.pdf

Goddard, A. S., and Carrapa, B. (2018). Effects of Miocene-Pliocene global climate changes on continental sedimentation: a case study from the southern Central Andes. *Geology* 46, 647–650. doi: 10.1130/G40280.1

Gorring, M., Singer, B., Gowers, J., and Kay, S. M. (2003). Plio–Pleistocene basalts from the Meseta del Lago Buenos Aires, Argentina: evidence for asthenosphere–lithosphere interactions during slab window magmatism. *Chem. Geol.* 193, 215–235. doi: 10.1016/s0009-2541(02)00249-8

Guillaume, B., Gautheron, C., Simon-Labric, T., Martinod, J., Roddaz, M., and Douville, E. (2013). Dynamic topography control on Patagonian relief evolution as inferred from low temperature thermochronology. *Earth Planet. Sci. Lett.* 364, 157–167. doi: 10.1016/j.epsl.2012.12.036

Guillaume, B., Martinod, J., Husson, L., Roddaz, M., and Riquelme, R. (2009). Neogene uplift of central eastern Patagonia: dynamic response to active spreading ridge subduction? *Tectonics* 28:55.

Heller, P. L., Angevine, C. L., Winslow, N. S., and Paola, C. (1988). Two-phase stratigraphie model of foreland-basin sequences. *Geology* 16, 501–504.

Heller, P. L., Burns, B., and Marzo, M. (1993). Stratographic solution sets for determining the roles of sediment supply, subsidence, and sea-level on transgressions and regressions. *Geology* 21, 747–750.

Heller, P. L., Paola, C., Hwang, I., John, B., and Steel, R. (2001). Geomorphology and sequence stratigraphy due to slow and rapid base-level changes in an experimental subsiding Basin (XES 96-1). *Am. Assoc. Petrol. Geol. Bull.* 85, 817–838. doi: 10.1306/8626CA0F-173B-11D7-8645000102C1865D

Hervé, F., Calderón, M., and Faúndez, V. (2008). The metamorphic complexes of the Patagonian and Fuegian Andes. *Geol. Acta* 6, 43–53.

Hervé, F., Fanning, C. M., and Pankhurst, R. J. (2003). Detrital zircon age patterns and provenance of the metamorphic complexes of southern Chile. *J. South Am. Earth Sci.* 16, 107–123. doi: 10.1016/S0895-9811(03)00022-1

Hervé, F., Pankhurst, R. J., Fanning, C. M., Calderón, M., and Yaxley, G. M. (2007). The South Patagonian batholith: 150 my of granite magmatism on a plate margin. *Lithos* 97, 373–394. doi: 10.1016/j.lithos.2007.01.007

Hilley, G. E., Blisniuk, P. M., and Strecker, M. R. (2005). Mechanics and erosion of basement-cored uplift provinces. *J. Geophys. Res.* 110, 1–22. doi: 10.1029/2005JB003704

Horton, B. K. (1999). Erosional control on the geometry and kinematics of thrust belt development in the central Andes. *Tectonics* 18, 1292–1304. doi: 10.1029/1999TC900051

Horton, B. K. (2018). Sedimentary record of Andean mountain building. *Earth Sci. Rev.* 178, 279–309. doi: 10.1016/j.earscirev.2017.11.025

Horton, B. K., Constenius, K. N., and DeCelles, P. G. (2004). Tectonic control on coarse-grained foreland-basin sequences: an example from the Cordilleran foreland basin, Utah. *Geology* 32, 637–640. doi: 10.1130/G20407.1

Howard, J. L. (1993). The statistics of counting clasts in rudites: a review, with examples from the upper Palaeogene of southern California, USA. *Sedimentology* 40, 157–174. doi: 10.1111/j.1365-3091.1993.tb01759.x

Hubbard, S. M., Romans, B. W., and Graham, S. A. (2008). Deep-water foreland basin deposits of the cerro toro formation, Magallanes basin, Chile: architectural elements of a sinuous basin axial channel belt. *Sedimentology* 55, 1333–1359. doi: 10.1111/j.1365-3091.2007.00948.x

Hünicken, M. (1955). Depósitos neocretácicos y terciarios del extremo S.S.W. de Santa Cruz. Cuenca Carbonífera de Río Turbio. *Rev. Instit. Nacl. Invest. Cienc. Nat.* 4, 1–161.

Ingersoll, R. V., Bullard, T. F., Ford, R. L., Grimm, J. P., Pickle, J. D., and Sares, S. W. (1984). The effect of grain size of detrital modes: a test of the Gazzi-Dickinson point-counting method. *J. Sediment. Res.* 54, 103–116. doi: 10.1306/212F83B9-2B24-11D7-8648000102C1865D

Johnsson, M. J. (1993). The system controlling the composition of clastic sediments. *Geol. Soc. Am. Special Pap.* 284, 1–19.

Jordan, T., Allmendinger, R., Damanti, J., and Drake, R. (1993). Chronology of motion in a complete thrust belt: the Precordillera, 30-31°S, Andes Mountains. *J. Geol.* 101, 135–156. doi: 10.1086/648213

Jordan, T. E., and Flemings, P. B. (1991). Large-scale stratigraphic architecture, eustatic variation, and unsteady tectonism: a theoretical evaluation. *J. Geophys. Res.* 96, 6681–6699. doi: 10.1038/ncomms11427

Kay, S. M., Gorring, M., and Ramos, V. A. (2004). Magmatic sources, setting and causes of Eocene to Recent Patagonian plateau magmatism (36°S to 52 °S latitude). *Rev. Asoc. Geol. Argent.* 59, 556–568.

Lagabrielle, Y., Goddéris, Y., Donnadieu, Y., Malavieille, J., and Suarez, M. (2009). The tectonic history of Drake Passage and its possible impacts on global climate.

Earth and Planetary Science Letters 279, 197–211. doi: 10.1016/j.epsl.2008.12.037

Macellari, C. E., Barrio, C. A., and Manassero, M. J. (1989). Upper Cretaceous to Paleocene depositional sequences and standstone petrography of southwestern Patagonia (Argentina and Chile). *J. South Am. Earth Sci.* 2, 223–239. doi: 10.1016/0895-9811(89)90031-x

Malkowski, M. A., Sharman, G. R., Graham, S. A., and Fildani, A. (2017). Characterization and diachronous initiation of coarse clastic deposition in the Magallanes–Austral foreland basin, Patagonian Andes. *Basin Res.* 29, 298–326. doi: 10.1111/bre.12150

Malumián, N., and Caramés, A. (1997). Upper Campanian-Paleogene from the Río Turbio coal measures in southern Argentina: micropaleontology and the Paleocene/Eocene boundary. *J. South Am. Earth Sci.* 10, 189–201. doi: 10.1016/s0895-9811(97)00015-1

Malumián, N., and Náñez, C. (2011). Late Cretaceous-Cenozoic transgressions in Patagonia and the Fuegian Andes: foraminifera, paleoecology, and paleogeography. *Biol. J. Linnean Soc.* 103, 269–288. doi: 10.1111/j.1095-8312.2011.01649.x

Malumián, N., Panza, J. L., Parisi, C., Naňez, C., Caramés, A., and Torre, A. (2000). Hoja Geológica 5172-III, Yacimiento Río Turbio (1:250,000). *Serv. Geol. Minero Argent. Boletin* 247, 180.

Manassero, M. J. (1990). *Composición y procedencia de la Formación Río Turbio en el sector occidental del Valle Homónimo, Provincia de Santa Cruz: III Reunión Argentina de Sedimentología* (San Juan: Resúmenes), 181–186.

Miall, A. D. (1978). "Lithofacies types and vertical profile models in braided river deposits: a summary," in *Fluvial Sedimentology*, ed. A. D. Miall, (Calgary: Canadian Society of Petroleum Geology), 597–604.

Miall, A. D. (2006). *The Geology of Fluvial Deposits: Sedimentary Facies, Analysis and Petroleum Geology*. New York, NY: Spring-Verlag.

Michel, J., Baumgartner, L., Putlitz, B., Schaltegger, U., and Ovtcharova, M. (2008). Incremental growth of the Patagonian Torres del Paine laccolith over 90 k.y. *Geology* 36, 459–462. doi: 10.1130/G24546A.1

Miller, K. G., Kominz, M. A., Browning, J. V., Wright, J. D., Mountain, G. S., Katz, M. E., et al. (2005). The Phanerozoic record of global sea-level change. *Science* 310, 1293–1298. doi: 10.1126/science.1116412

Mora, A., Parra, M., Strecker, M. R., Kammer, A., Dimaté, C., and Rodríguez, F. (2006). Cenozoic contractional reactivation of Mesozoic extensional structures in the Eastern Cordillera of Colombia. *Tectonics* 25, 1–19. doi: 10.1029/2005TC001854

Paola, C. (2000). Quantitative models of sedimentary basin filling. *Sedimentology* 41, 121–178. doi: 10.1046/j.1365-3091.2000.00006.x

Paola, C., Heller, P. L., and Angevine, C. L. (1992). The large-scale dynamics of grain-size variation in alluvial basins, 1: theory. *Basin Res.* 4, 73–90. doi: 10.1111/j.1365-2117.1992.tb00145.x

Parras, A., Dix, G. R., and Griffin, M. (2012). Sr-isotope chronostratigraphy of Paleogene-Neogene marine deposits: Austral Basin, southern Patagonia (Argentina). *J. South Am. Earth Sci.* 37, 122–135. doi: 10.1016/j.jsames.2012.02.007

Parras, A., Griffin, M., Feldmann, R., Casadío, S., Schweitzer, C., and Marenssi, S. (2008). Journal of South American Earth Sciences Correlation of marine beds based on Sr- and Ar-date determinations and faunal affinities across the Paleogene/Neogene boundary in southern Patagonia, Argentina. *J. South Am. Earth Sci.* 26, 204–216. doi: 10.1016/j.jsames.2008.03.006

Pearson, N. J., Mángano, M. G., Buatois, L. A., Casadío, S., and Rodríguez Raising, M. (2012). Ichnology, sedimentology, and sequence stratigraphy of out-estuarine and coastal-plain deposits: implications for the distinction between allogenic and autogenic expressions of the Glossifungites Ichnofacies. *Paleogeogr. Paleoclimatol. Paleoecol.* 333, 192–217. doi: 10.1016/j.paleo.2012.03.031

Posamentier, H. W., Jervey, M. T., and Vail, P. R. (1988). "Eustatic controls on clastic deposition I - conceptual framework," in *Sea Level Changes - An Integrated Approach, Special Publication*, eds C. K. Wilgus, B. S. Hastings, C.G. St. C. Kendall, H. W. Posamentier, C. A. Ross, and J. C. Van Wagoner, (Tulsa: Society of Economic Paleontologists and Minerologists), 110–124.

Ramírez de Arellano, C., Putlitz, B., Müntener, O., and Ovtcharova, M. (2012). High precision U/Pb zircon dating of the Chaltén Plutonic Complex (Cerro Fitz Roy, Patagonia) and its relationship to arc migration in the southernmost Andes. *Tectonics* 31:C003048.

Ramos, V. A. (1989). Andean foothills structures in Northern Magallanes Basin, Argentina. *Am. Assoc. Petrol. Geol. Bull.* 73, 887–903.

Ramos, V. A., and Kay, S. M. (1992). Southern Patagonian plateau basalts and deformation: backarc testimony of ridge collisions. *Tectonophysics* 205, 261–282. doi: 10.1016/0040-1951(92)90430-E

Ramos, V. R., and Ghiglione, M. C. (2008). Tectonic evolution of the Patagonian Andes. *Dev. Quat. Sci.* 11, 57–71. doi: 10.1016/s1571-0866(07)10004-x

Riccardi, A. C., and Rolleri, E. O. (1980). *Cordillera Patagonica Austral, Segundo Simosio Geología Regional Argentina*. La Paz: Acadmia Nacional de Ciencias, 1174–1306.

Rodríguez Raising, M. (2010). *Estratigrafía Secuencial de los Depósitos Marinos y Continentales del Eoceno – Oligoceno Temprano de la Cuenca Austral, Suroeste de la Provincia de Santa Cruz*. Ph.D. thesis, Cuenca austral, Santa Cruz.

Romans, B. W., Castelltort, S., Covault, J. A., Fildani, A., and Walsh, J. P. (2016). Environmental signal propagation in sedimentary systems across timescales. *Earth Sci. Rev.* 153, 7–29. doi: 10.1016/j.earscirev.2015.07.012

Romans, B. W., Fildani, A., Graham, S. A., Hubbard, S. M., and Covault, J. A. (2010). Importance of predecessor basin history on the sedimentary fill of a retroarc foreland basin: provenance analysis of the Cretaceous Magallanes. *Basin Res.* 22, 640–658. doi: 10.1111/j.1365-2117.2009.00443.x

Romans, B. W., Fildani, A., Hubbard, S. M., Covault, J. A., Fosdick, J. C., and Graham, S. A. (2011). Evolution of deep-water stratigraphic architecture, Magallanes Basin, Chile. *Mar. Petrol. Geol.* 28, 612–628. doi: 10.1016/j.marpetgeo.2010.05.002

Russo, A., Flores, M. A., and Di Benedetto, H. (1980). *Patagonia Austral Extraandina: Segundo Simosio Geología Regional Argentina* (La Paz: Acadmia Nacional de Ciencias), 1431–1462.

Sánchez, A., Hervé, F., and de Saint-blanquat, M. (2008). "Relations between plutonism in the back-arc region in southern Patagonia and Chile Rise subduction: a geochronological review," in *Proceddings of the 7th international Symposium on Andean Geodynamics (ISAG 2008, Nice)*, (Oxford: John Wiley & Sons), 485–488.

Saylor, J. E., Horton, B. K., Stockli, D. F., Mora, A., and Corredor, J. (2012). Structural and thermochronological evidence for Paleogene basement-involved shortening in the axial Eastern Cordillera, Colombia. *J. South Am. Earth Sci.* 39, 202–215. doi: 10.1016/j.jsames.2012.04.009

Schwartz, T. M., Fosdick, J. C., and Graham, S. A. (2016). Using detrital zircon U-Pb ages to calculate Late Cretaceous sedimentation rates in the Magallanes-Austral basin, Patagonia. *Basin Res.* 29, 725–746. doi: 10.1111/bre.12198

Schwartz, T. M., and Graham, S. A. (2015). Stratigraphic architecture of a tide-influenced shelf-edge delta, Upper Cretaceous Dorotea Formation, Magallanes-Austral Basin, Patagonia. *Sedimentology* 62, 1039–1077. doi: 10.1111/sed.12176

SERNAGEOMIN (2003). *Mapa Geológico de Chile: Version Digital. Publicación Geológica Digital, No. 4, 2003. CDROM, version 1.0, 2003. Base Geológica escala 1:1.000.000*. Santiago: Servicio Nacional de Geología y Minería.

Sickmann, Z. T., Schwartz, T. M., Malkowski, M. A., Dobbs, S. C., and Graham, S. A. (2019). Interpreting large detrital geochronology data sets in retroarc foreland basins: an example from the Magallanes-Austral Basin, southernmost Patagonia. *Lithosphere2* 11, 620–642. doi: 10.1130/L1060.1/4792995/l1060.pdf

Somoza, R., and Ghidella, M. E. (2012). Late Cretaceous to recent plate motions in western South America revisited. *Earth Planet. Sci. Lett.* 331, 152–163. doi: 10.1016/j.epsl.2012.03.003

Thomson, S. N., Hervé, F., and Stöckhert, B. (2001). Mesozoic-Cenozoic denudation history of the Patagonian Andes (southern Chile) and its correlation to different subduction precesses. *Tectonics* 20, 693–711. doi: 10.1029/2001TC900013

VanderLeest, R. A., Fosdick, J. C., Leonard, J. S., and Morgan, L. E. (2018). "Early miocene mafic arc volcanism of the patagonian andes revealed with detrital multi-chronometer and trace element geochemistry from the Magallanes Basin 50-52°," in *Proceedings of the American Geophysical Union Fall Meeting 2018*, (Washington, D.C: American Geophysical Union).

Varela, A. N., Gomez-Peral, L. E., Richiano, S., and Poiré, D. G. (2013). Distinguishing similar volcanic source areas from an integrated provenance analysis: implications for foreland Andean basins. *J. Sedimentary Res.* 83, 258–276. doi: 10.2110/jsr.2013.22

Valenzuela, A. (2006). *Provenienca Sedimentaria de Estratos de Cabo Nariz y Formacion Cerro Toro, Cretacico Tardio - Paleoceno, Magallanes, Chile*. Ph.D. thesis, Universidad de Chile, Santiago.

Willett, S. D. (1999). Orogeny and orography: the effects of erosion on the structure of mountain belts. *J. Geophys. Res.* 104, 28957–28987. doi: 10.1029/1999JB900248

Wilson, T. J. (1991). Transition from back-arc to foreland basin development in the southernmost andes - stratigraphic record from the Ultima-Esperanza-District, Chile. *Geol. Soc. Am. Bull.* 103, 98–111. doi: 10.1130/0016-7606(1991)103<0098:tfbatf>2.3.co;2

Conflict of Interest: The authors declare that the research was conducted in the absence of any commercial or financial relationships that could be construed as a potential conflict of interest.